

Do quasar X-ray and UV flux measurements provide a useful test of cosmological models?

Narayan Khadka,^{id}¹★ Bharat Ratra^{id}¹†

¹Department of Physics, Kansas State University, 116 Cardwell Hall, Manhattan, KS 66502, USA

Accepted XXX. Received YYY; in original form ZZZ

ABSTRACT

The recent compilation of quasar (QSO) X-ray and UV flux measurements include QSOs that appear to not be standardizable via the X-ray luminosity and UV luminosity ($L_X - L_{UV}$) relation and so should not be used to constrain cosmological model parameters. Here we show that the largest of seven sub-samples in this compilation, the SDSS-4XMM QSOs that contribute about 2/3 of the total QSOs, have $L_X - L_{UV}$ relations that depend on the cosmological model assumed and also on redshift, and is the main cause of the similar problem discovered earlier for the full QSO compilation. The second and third biggest sub-samples, the SDSS-Chandra and XXL QSOs that together contribute about 30% of the total QSOs, appear standardizable, but provide only weak constraints on cosmological parameters that are not inconsistent with the standard spatially-flat Λ CDM model or with constraints from better-established cosmological probes.

Key words: (cosmology:) cosmological parameters – (cosmology:) observations – (cosmology:) dark energy

1 INTRODUCTION

Currently our universe is undergoing accelerated cosmological expansion (eBOSS Collaboration 2021; Farooq et al. 2017; Planck Collaboration 2020; Scolnic et al. 2018). General relativistic cosmological models interpret this observational fact as a consequence of dark energy. The simplest cosmological model that is consistent with most observations is the standard spatially-flat Λ CDM model (Peebles 1984). In this model, at the current epoch, the cosmological constant (Λ) contributes about 70% of the cosmological energy budget, non-relativistic cold dark matter (CDM) contributes about 25%, and ordinary non-relativistic baryons contributes almost all of the remaining $\sim 5\%$. This model assumes time-independent dark energy density and flat spatial hypersurfaces and is not inconsistent with most observational constraints.¹ However, observational data do not rule out a small amount of spatial curvature nor do they rule out mildly dynamical dark energy. So in this paper we also consider spatially non-flat models and dynamical dark energy models.

Cosmological models are largely tested using low and high redshift data. The low redshift data probe the $0 \leq z \leq 2.3$ part of cosmological redshift space and include baryon acoustic oscillation (BAO), Hubble parameter [$H(z)$], and Type Ia supernova (SNIa) apparent magnitude measurements. The only high cosmological

redshift space probe are cosmic microwave background anisotropy data at $z \sim 1100$. In the intermediate redshift range, $2.3 < z < 1100$, cosmological models are poorly tested. There are a handful of astronomical data sets in this range that are starting to be used in cosmology. These data sets include HII starburst galaxy observations reaching to $z \sim 2.4$ (Mania & Ratra 2012; Chávez et al. 2014; González-Morán et al. 2019, 2021; Cao et al. 2020, 2021c,a; Johnson et al. 2021), quasar (QSO) angular size observations reaching to $z \sim 2.7$ (Cao et al. 2017; Ryan et al. 2019; Cao et al. 2020, 2021d; Zheng et al. 2021; Lian et al. 2021), gamma-ray burst observations reaching to $z \sim 8.2$ (Amati et al. 2008, 2019; Samushia & Ratra 2010; Wang et al. 2016, 2021; Demianski et al. 2019; Fana Dirirsa et al. 2019; Khadka & Ratra 2020c; Khadka et al. 2021a; Cao et al. 2021b), and recently Vagnozzi et al. (2021a) has used old astrophysical objects in the redshift range $0 \leq z \leq 8$ to constrain cosmological parameters.

Quasar X-ray and UV flux observations reaching to $z \sim 7.5$ (Risaliti & Lusso 2015, 2019; Lusso et al. 2020) is another such data set that could be used to constrain cosmological model parameters.² QSO X-ray and UV luminosities are correlated through a non-linear relation, the $L_X - L_{UV}$ relation $L_X = 10^\beta L_{UV}^\gamma$ where β and γ

* E-mail: nkhadka@phys.ksu.edu

† E-mail: ratra@phys.ksu.edu

¹ For recent reviews see Di Valentino et al. (2021a) and Perivolaropoulos & Skara (2021).

² For recent applications and discussions of these data see Yang et al. (2020), Wei & Melia (2020), Lindner et al. (2020), Khadka & Ratra (2020a,b, 2021), Rezaei et al. (2020), Hu et al. (2020), Banerjee et al. (2021) Speri et al. (2021), Zheng et al. (2021), Zhao & Xia (2021), Li et al. (2021), Lian et al. (2021), and references therein.

Table 1. Subsets of the full QSO (2421 QSOs) data compilation.

Data set	Redshift range	Number of QSOs
SDSS-4XMM	$0.131 \leq z \leq 3.412$	1644
SDSS-Chandra	$0.489 \leq z \leq 3.981$	608
XXL	$0.2436 \leq z \leq 1.9247$	106
Local AGN	$0.009 \leq z \leq 0.0866$	13
High- z	$4.01 \leq z \leq 7.5413$	35
XMM-Newton~3	$3.028 \leq z \leq 3.296$	14
XMM-Newton~4	4.109	1

are parameters. This correlation enables us to standardize and so use these QSO data³ to derive cosmological parameter constraints. Basic assumptions underlying the use of the $L_X - L_{UV}$ relation for the standardization of QSO data are: (i) the $L_X - L_{UV}$ relation parameters, intercept (β) and slope (γ), should not evolve with redshift; and, (ii) these parameters should be independent of the cosmological model used to measure them. While great effort has been made to standardize these QSO data using the $L_X - L_{UV}$ relation the most recent QSO data compilation of Lusso et al. (2020) violate both assumptions underpinning QSO standardization via the $L_X - L_{UV}$ relation (Khadka & Ratra 2021). So at least some of the QSOs in the Lusso et al. (2020) compilation are not standardizable through the $L_X - L_{UV}$ relation. These QSO data are a possibly heterogeneous compilation of seven different sub-samples that are summarized in Table 1. In this paper, we study these QSO data more granularly to try to determine whether some of the sub-samples are more responsible for the redshift-dependent and model-dependent behavior of β and γ values discovered by Khadka & Ratra (2021).

The largest sub-sample in the Lusso et al. (2020) QSO compilation are SDSS-4XMM QSOs. Our analyses here show that the β and γ values measured for this sub-sample depend on the cosmological model used and change with redshift. On the other hand, other large sub-samples, such as SDSS-Chandra QSOs, have model-independent β and γ values. So the main issues are mostly related with the SDSS-4XMM QSOs and these need to be resolved if these QSOs are to be used for cosmological purposes. We note that there has been a recent claim of a larger than 4σ tension between these QSO data and the standard spatially-flat Λ CDM model with $\Omega_{m0} = 0.3$ (Lusso et al. 2020). We believe that this is more properly interpreted as an indirect indication that these QSOs are not standard candles and so cannot be used for cosmological purposes (Khadka & Ratra 2021). While we have discovered an issue with the SDSS-4XMM data, it is at present not known if this was generated during the original compilation process or whether the SDSS-4XMM QSOs have an $L_X - L_{UV}$ relation that evolves with z and so are non-standardizable. We also note that other, somewhat lower z , reverberation-measured Mg II, radius-luminosity standardized, QSO constraints are consistent with the standard flat Λ CDM model (Martínez-Aldama et al. 2019; Czerny et al. 2021; Zajaček et al. 2021; Yu et al. 2021; Khadka et al. 2021b).

Our paper is organized as follows. In Sec. 2 we describe the cosmological models we study. In Sec. 3 we summarize the data sub-sets, and compilations of these, that we analyze. In Sec. 4 we describe analysis methods we use. We present our results in Sec. 5 and conclude in Sec. 6.

³ We can employ the $L_X - L_{UV}$ relation to measure the luminosity distance or distance modulus of quasars that obey this correlation. So if the $L_X - L_{UV}$ correlation relation is valid these quasars are standard candles.

2 MODELS

To constrain cosmological model parameters we compare model predictions, that depend on these parameters, to measurements made at known redshifts. So as to understand how model-dependent our results are, we consider six different models, three with non-flat spatial hypersurfaces and three with flat spatial hypersurfaces.⁴ For the observables we study in this paper, the model predictions are determined by the Hubble parameter, the cosmological expansion rate, that is a function of the redshift z and the parameters of the cosmological model.

In these six cosmological models the Hubble parameter is

$$H(z) = H_0 \sqrt{\Omega_{m0}(1+z)^3 + \Omega_{k0}(1+z)^2 + \Omega_{DE}(z)}. \quad (1)$$

Here H_0 is the Hubble constant, Ω_{m0} and Ω_{k0} are the current values of the non-relativistic matter and curvature energy density parameters, and $\Omega_{DE}(z)$ is the dark energy density parameter. $\Omega_{k0} = 0$ in the spatially-flat models. We consider three different models of dark energy. In two of the three models we study, the dark energy density evolves as a power of $(1+z)$: $\Omega_{DE}(z) = \Omega_{DE0}(1+z)^{1+\omega_X}$ where Ω_{DE0} is the current value of the dark energy density parameter and ω_X is the dark energy equation of state parameter (see below).

In the Λ CDM model dark energy is the standard cosmological constant with $\omega_X = -1$ and $\Omega_{DE} = \Omega_{DE0} = \Omega_\Lambda$. The current values of the three Λ CDM model energy density parameters are constrained by the energy budget equation $\Omega_{m0} + \Omega_{k0} + \Omega_\Lambda = 1$. In the spatially-flat Λ CDM model Ω_{m0} is picked to be the free parameter while in the non-flat Λ CDM model Ω_{m0} and Ω_{k0} are the free parameters.

In the XCDM parametrization dark energy is the ideal parametrized X -fluid with equation of state parameter ω_X (the ratio of the X -fluid pressure and energy density) and $\Omega_{DE0} = \Omega_{X0}$ is the current value of the dynamical X -fluid dark energy density parameter. The current values of the three XCDM parametrization energy density parameters are constrained by the energy budget equation $\Omega_{m0} + \Omega_{k0} + \Omega_{X0} = 1$. When $\omega_X > -1$ the X -fluid dark energy density decreases with time. In the spatially-flat XCDM parametrization Ω_{m0} and ω_X are the free parameters while in the non-flat XCDM parametrization, Ω_{m0} , Ω_{k0} , and ω_X are picked to be the free parameters. When $\omega_X = -1$ the XCDM parametrization reduces to the Λ CDM model.

In the ϕ CDM model (Peebles & Ratra 1988; Ratra & Peebles 1988; Pavlov et al. 2013) dynamical dark energy is a scalar field ϕ and the dynamical dark energy density parameter Ω_{DE} depends on the scalar field potential energy density.⁵ We assume an inverse power law scalar field potential energy density

$$V(\phi) = \frac{1}{2} k m_p^2 \phi^{-\alpha}, \quad (2)$$

where m_p is the Planck mass, α is a positive parameter [$\Omega_{DE} =$

⁴ For spatial curvature observational constraints see Farooq et al. (2015), Chen et al. (2016), Rana et al. (2017), Yu et al. (2018), Ooba et al. (2018a,c), Wei (2018), Park & Ratra (2019c,a), DES Collaboration (2019), Handley (2019), Li et al. (2020), Efstathiou & Gratton (2020), Di Valentino et al. (2021b), Velasquez-Toribio & Fabris (2020), Vagnozzi et al. (2020, 2021b), KiDS Collaboration (2021), Arjona & Nesseris (2021), Dhawan et al. (2021), and references therein.

⁵ For ϕ CDM model observational constraints see Avsajianishvili et al. (2015), Ryan et al. (2018), Solà Peracaula et al. (2018, 2019), Zhai et al. (2017), Ooba et al. (2018b, 2019), Park & Ratra (2018, 2019b, 2020), Sangwan et al. (2018), Singh et al. (2019), Ureña-López & Roy (2020), Sinha & Banerjee (2021), and references therein.

$\Omega_\phi(z, \alpha)$ is the dynamical dark energy density parameter], and the constant κ is determined by ensuring that, in the numerical integration, the current energy budget constraint $\Omega_{m0} + \Omega_{k0} + \Omega_\phi(z = 0, \alpha) = 1$ is satisfied.

With the potential energy density of eq. (2), the equations of motion for a spatially homogeneous scalar field and metric tensor are

$$\ddot{\phi} + 3\frac{\dot{a}}{a}\dot{\phi} - \frac{1}{2}\alpha\kappa m_p^2\phi^{-\alpha-1} = 0, \quad (3)$$

$$\left(\frac{\dot{a}}{a}\right)^2 = \frac{8\pi}{3m_p^2}(\rho_m + \rho_\phi) - \frac{k}{a^2}. \quad (4)$$

Here an overdot denotes a derivative with respect to time, a is the scale factor, ρ_m is the non-relativistic matter energy density, for open, flat, and closed spatial hypersurfaces the curvature index k is negative, zero, and positive (corresponding to $\Omega_{k0} > 0, = 0$, and < 0), and the scalar field energy density

$$\rho_\phi = \frac{m_p^2}{32\pi}[\dot{\phi}^2 + \kappa m_p^2\phi^{-\alpha}]. \quad (5)$$

By numerically integrating eqs. (3) and (4), we compute ρ_ϕ , and then determine $\Omega_\phi(z, \alpha)$ by using

$$\Omega_\phi(z, \alpha) = \frac{8\pi\rho_\phi}{3m_p^2H_0^2}. \quad (6)$$

In the spatially-flat ϕ CDM model Ω_{m0} and α are the free parameters while in the non-flat ϕ CDM model, Ω_{m0} , Ω_{k0} , and α are picked to be the free parameters. When $\alpha = 0$ the ϕ CDM model reduces to the Λ CDM model.

3 DATA

We use the better 2036 (of 2421) QSOs sample⁶ from the Lusso et al. (2020) compilation. These better QSO data consist of seven different QSO sub-samples that are listed in Table 2. In Khadka & Ratra (2021) we discovered that the $L_X - L_{UV}$ relation parameters for the complete better QSO sample are model dependent as well as redshift dependent. This means that some of the QSOs in the complete sample are not standardizable through the $L_X - L_{UV}$ relation. In this paper, we analyse the individual QSO sub-samples, as well as some combinations of these sub-samples, in an attempt to determine which QSO sub-samples are more responsible for the problem we discovered in Khadka & Ratra (2021). In addition to the larger individual sub-samples of Table 2, we also consider combinations of sub-samples that are listed in Table 3. In all, we study 11 different QSO sub-samples, the eight sub-samples listed in Table 3 and the SDSS-4XMM, SDSS-Chandra, and XXL sub-samples of Table 2.

In this paper, we also use constraints on cosmological parameters obtained from joint analyses of 11 BAO and 31 $H(z)$ measurements to compare with the cosmological constraints obtained using the QSO sub-groups. These data are described in Khadka & Ratra (2021).

⁶ For some of the QSOs at $z < 0.7$ in the 2421 QSO sample the 2500 Å UV flux was determined by extrapolation from the optical which is less reliable because of possible host-galaxy contamination (Lusso et al. 2020) and so these QSOs are excluded from the 2036 QSO sample.

Table 2. Subsets of the better QSO (2036 QSOs) data compilation.

Data set	Redshift range	Number of QSOs
SDSS-4XMM	$0.703 \leq z \leq 3.412$	1355
SDSS-Chandra	$0.7031 \leq z \leq 3.981$	542
XXL	$0.7061 \leq z \leq 1.9247$	76
Local AGN	$0.009 \leq z \leq 0.0866$	13
High- z	$4.01 \leq z \leq 7.5413$	35
XMM-Newton~3	$3.028 \leq z \leq 3.296$	14
XMM-Newton~4	4.109	1

Table 3. Combinations of subsets of better QSO (2036 QSOs) data.

Data set	Redshift range	Number of QSOs
SDSS-4XMM-I ^a	$0.703 \leq z \leq 1.4615$	678
SDSS-4XMM-h ^b	$1.4655 \leq z \leq 3.412$	677
Chandra + Newton-3	$0.7031 \leq z \leq 3.981$	556
High- z + Newton-4	$4.01 \leq z \leq 7.5413$	36
Chandra + XXL	$0.7031 \leq z \leq 3.981$	618
Chandra + High- z + Newton-4	$0.7031 \leq z \leq 7.5413$	578
Chandra + XXL + Newton-3	$0.7031 \leq z \leq 3.981$	632
QSO ^c	$0.7031 \leq z \leq 7.5413$	668

^a Lower z half of SDSS-4XMM.

^b Higher z half of SDSS-4XMM.

^c SDSS-Chandra + XXL + High- z + Newton-3 + Newton-4.

4 METHODS

The non-linear $L_X - L_{UV}$ relation relates the X-ray and UV luminosities of selected QSOs. This relation is

$$\log(L_X) = \beta + \gamma \log(L_{UV}), \quad (7)$$

where $\log = \log_{10}$ and γ and β are free parameters to be measured from the data.

If we express luminosities in terms of fluxes, eq. (7) becomes

$$\log(F_X) = \beta + (\gamma - 1)\log(4\pi) + \gamma \log(F_{UV}) + 2(\gamma - 1)\log(D_L). \quad (8)$$

Here F_X and F_{UV} are the quasar X-ray and UV fluxes and $D_L(z, p)$ is the luminosity distance. The luminosity distance can be computed in each cosmological model at a given redshift z and for a given set of cosmological model parameters p ,

$$H_0\sqrt{|\Omega_{k0}|}D_L(z, p) = \begin{cases} \sinh[g(z)] & \text{if } \Omega_{k0} > 0, \\ g(z) & \text{if } \Omega_{k0} = 0, \\ \sin[g(z)] & \text{if } \Omega_{k0} < 0, \end{cases} \quad (9)$$

where

$$g(z) = H_0\sqrt{|\Omega_{k0}|} \int_0^z \frac{dz'}{H(z')}, \quad (10)$$

and $H(z)$ is a Hubble parameter described in Sec. 2 for each model we study.

Once we compute predicted X-ray fluxes using eqs. (8) and (9) in a given model, we compare these predicted fluxes with observations by using the likelihood function (D'Agostini 2005)

$$\ln(\text{LF}) = -\frac{1}{2} \sum_{i=1}^N \left[\frac{[\log(F_{X,i}^{\text{obs}}) - \log(F_{X,i}^{\text{th}})]^2}{s_i^2} + \ln(2\pi s_i^2) \right]. \quad (11)$$

Here $\ln = \log_e$, $s_i^2 = \sigma_i^2 + \delta^2$, where σ_i and δ are the measurement

Table 4. Non-zero flat prior parameter ranges.

Parameter	Prior range
$\Omega_b h^2$	[0, 1]
$\Omega_c h^2$	[0, 1]
Ω_{m0}	[0, 1]
Ω_{k0}	[-2, 2]
ω_X	[-5, 0.33]
α	[0, 10]
δ	[0, 10]
β	[0, 11]
γ	[-5, 5]

error on the observed flux $F_{X,i}^{\text{obs}}$ and the global intrinsic dispersion⁷ respectively, and $F_{X,i}^{\text{th}}(p)$ is the predicted flux at redshift z_i . In the $L_X - L_{UV}$ relation, β and H_0 are degenerate so QSO data alone cannot constrain H_0 . We allow H_0 to be a free parameter to determine the complete allowed range of β . To avoid the QSO data circularity problem we simultaneously determine the $L_X - L_{UV}$ relation parameters and the cosmological model parameters when analyzing data. By studying a number of different cosmological models we are able to determine whether the $L_X - L_{UV}$ relation parameters are independent of the cosmological model in which they were measured. If the parameters of the $L_X - L_{UV}$ relation depend on the cosmological model then the corresponding QSOs are not standardized candles and so cannot be used for cosmological parameter estimation.

The BAO + $H(z)$ data constraints used in this paper are from Khadka & Ratra (2021). A detailed description of the method used for these data is given in Sec. 4 of Khadka & Ratra (2021).

We use the Markov chain Monte Carlo (MCMC) method, as implemented in the MONTEPYTHON code (Brinckmann & Lesgourges 2019), to perform the likelihood analyses. For each free parameter, we use the Gelman-Rubin criterion ($R - 1 < 0.05$) to determine the convergence of the MCMC chains. For each of the free parameter we use a flat prior non-zero over the range listed in Table 4.

5 RESULTS

The BAO + $H(z)$ data results are listed in Table 5. These are from Khadka & Ratra (2021) and are discussed in Sec. 5.3 of that paper. In this paper we use these BAO + $H(z)$ results to compare with the cosmological constraints obtained using the QSO sub-group samples to see whether the QSO sub-group sample results are consistent or not with the better-established BAO + $H(z)$ ones. These BAO + $H(z)$ results are shown in red in all figures. Results for QSO sub-group samples are given in Table 5. The QSO one-dimensional likelihood distributions and two-dimensional likelihood contours are shown in blue or green in Figs. 1–10.

The $L_X - L_{UV}$ relation parameters values depend on the QSO data sub-set studied. The intercept β ranges from $7.290^{+0.400}_{-0.400}$ to

$10.240^{+0.600}_{-0.600}$. The minimum value is obtained using the SDSS-4XMM QSO sample in the flat Λ CDM case while the maximum value is obtained using the SDSS-4XMM-h sample (the higher redshift half of the SDSS-4XMM sub-set) in the non-flat XCDM case. The difference between maximum and minimum values is 4.1σ and statistically significant. The slope γ ranges from $0.536^{+0.012}_{-0.019}$ to $0.630^{+0.013}_{-0.013}$. The minimum value is obtained using the SDSS-4XMM-h QSO sample in the non-flat XCDM case while the maximum value is obtained using the SDSS-4XMM QSO sample in the spatially-flat Λ CDM model. The difference between maximum and minimum values is 5.3σ and statistically significant. The intrinsic dispersion (δ) is the third free parameter of the $L_X - L_{UV}$ relation. For all data sub-sets, values of δ lie in the range ~ 0.2 – 0.24 .

The SDSS-4XMM and SDSS-Chandra sub-samples are large sub-sets containing 1355 and 542 QSOs respectively, and when one of these sub-groups is part of the data under analysis it effectively determines the $L_X - L_{UV}$ relation parameter values.

For the SDSS-4XMM QSOs, comparing β and γ values listed in the last two columns of Table 5 for each of the six cosmological models, we see that these are significantly model-dependent. This means that the $L_X - L_{UV}$ relation for the SDSS-4XMM QSOs depends on the cosmological model in which it is estimated. This indicates that current SDSS-4XMM QSOs are not standardizable through the $L_X - L_{UV}$ relation and so cannot be used for cosmological parameter estimation purposes. This is similar to the result found in Khadka & Ratra (2021) for the complete QSO sample. Given that the SDSS-4XMM sub-set is by far the largest QSO sub-set, our finding here establishes that the SDSS-4XMM sub-set is a significant driver of the earlier result for the complete QSO compilation (Khadka & Ratra 2021). The SDSS-4XMM QSO sample quantitative differences between β and γ values for different pairs of cosmological model are listed in Table 6. The difference between γ values ($\Delta\gamma$) from model to model ranges over $(0 - 3.54)\sigma$ which is statistically significant. The difference between β values ($\Delta\beta$) from model to model ranges over $(0 - 3.82)\sigma$ which is statistically significant.

In an attempt to track down the cause of this effect, we divide SDSS-4XMM QSOs into two sub-sets, the lower redshift half, SDSS-4XMM-l, with QSOs at $z \leq 1.4615$ and the higher redshift half, SDSS-4XMM-h, with QSOs at $z > 1.4615$. For a given cosmological model, these two data sub-sets give different β and γ values. The differences in β and γ values for the two data sub-sets, for six different cosmological models, are listed in Table 7. In the six models, the difference between γ values ($\Delta\gamma$) range over $(1.55 - 2.50)\sigma$ and that between β values ($\Delta\beta$) range over $(1.62 - 2.14)\sigma$. These are statistically significant and show that in their current form SDSS-4XMM QSOs in different redshift regions follow different $L_X - L_{UV}$ relations. Whether this is because the SDSS-4XMM QSO $L_X - L_{UV}$ relation physically evolves, or some other effect causes this, remains to be established. Another possibly significant result of our analyses of these lower and higher redshift sub-sets is that both low and high z SDSS-4XMM QSOs follow model-independent (but different) $L_X - L_{UV}$ relations. This can be seen from Tables 8 and 9. This indicates that narrower-redshift bins of SDSS-4XMM QSOs obey model-independent $L_X - L_{UV}$ relations and that possibly the model-dependency and the redshift-dependency of β and γ values for these are related.

⁷ The intrinsic dispersion of the $L_X - L_{UV}$ relation quantifies unaccounted errors in the measurements. The larger value of the intrinsic dispersion for current QSO data is one of the reasons they are unable to provide precise cosmological constraints. The source of this dispersion is unknown and could include quasar variability and unknown systematics in the measurements (Risaliti & Lusso 2015).

Table 5: Marginalized one-dimensional best-fit parameters with 1σ confidence intervals, or 2σ limits, for sub-groups of the 2036 better QSOs compilation.

Model	Data set	Ω_{m0}	Ω_{Λ^c}	Ω_{k0}	ω_X	α	H_0^a	δ	β	γ
Flat Λ CDM	SDSS-4XMM	> 0.772	< 0.228	-	-	-	-	$0.225^{+0.005}_{-0.005}$	$7.290^{+0.400}_{-0.400}$	$0.630^{+0.013}_{-0.013}$
	SDSS-Chandra	> 0.348	< 0.652	-	-	-	-	$0.238^{+0.008}_{-0.008}$	$8.190^{+0.540}_{-0.540}$	$0.602^{+0.018}_{-0.018}$
	XXL	-	-	-	-	-	-	$0.211^{+0.016}_{-0.016}$	$7.300^{+1.500}_{-1.500}$	$0.632^{+0.018}_{-0.018}$
	Chandra + Newton-3	> 0.350	< 0.650	-	-	-	-	$0.236^{+0.008}_{-0.008}$	$7.960^{+0.500}_{-0.500}$	$0.609^{+0.017}_{-0.017}$
	High- z + Newton-4	-	-	-	-	-	-	$0.198^{+0.034}_{-0.034}$	$9.250^{+0.560}_{-0.560}$	$0.575^{+0.015}_{-0.015}$
	Chandra + XXL	> 0.378	< 0.622	-	-	-	-	$0.234^{+0.008}_{-0.008}$	$8.070^{+0.510}_{-0.510}$	$0.605^{+0.017}_{-0.017}$
	Chandra + High- z + Newton-4	> 0.435	< 0.565	-	-	-	-	$0.238^{+0.008}_{-0.008}$	$7.820^{+0.500}_{-0.500}$	$0.614^{+0.017}_{-0.017}$
	Chandra + XXL + Newton-3	> 0.350	< 0.650	-	-	-	-	$0.232^{+0.007}_{-0.007}$	$7.850^{+0.470}_{-0.470}$	$0.613^{+0.016}_{-0.016}$
	SDSS-4XMM-I	> 0.384	< 0.616	-	-	-	-	$0.233^{+0.007}_{-0.007}$	$8.000^{+0.680}_{-0.680}$	$0.606^{+0.016}_{-0.016}$
	SDSS-4XMM-h	> 0.360	< 0.640	-	-	-	-	$0.207^{+0.007}_{-0.006}$	$8.000^{+0.580}_{-0.580}$	$0.559^{+0.019}_{-0.019}$
	QSO ^b	> 0.522	< 0.478	-	-	-	-	$0.207^{+0.009}_{-0.009}$	$9.500^{+0.570}_{-0.570}$	$0.559^{+0.019}_{-0.019}$
	BAO + $H(z)$	> 0.462	< 0.538	-	-	-	-	$0.232^{+0.007}_{-0.007}$	$7.590^{+0.440}_{-0.440}$	$0.621^{+0.015}_{-0.015}$
	SDSS-4XMM	> 0.601	$1.704^{+0.069}_{-0.017}$	-	-	-	$69.300^{+1.800}_{-1.800}$	-	-	-
	SDSS-Chandra	$0.264^{+0.426}_{-0.084}$	$1.210^{+0.280}_{-0.033}$	$-0.660^{+0.250}_{-0.380}$	-	-	-	$0.236^{+0.008}_{-0.008}$	$9.070^{+0.700}_{-0.700}$	$0.574^{+0.023}_{-0.023}$
	XXL	-	-	< 1.700	$-0.018^{+1.188}_{-1.188}$	-	-	$0.212^{+0.016}_{-0.016}$	$7.400^{+1.500}_{-1.500}$	$0.626^{+0.026}_{-0.026}$
	Chandra + Newton-3	$0.247^{+0.393}_{-0.087}$	$1.250^{+0.230}_{-0.011}$	$-0.648^{+0.168}_{-0.322}$	-	-	-	$0.234^{+0.008}_{-0.008}$	$9.030^{+0.690}_{-0.690}$	$0.576^{+0.022}_{-0.022}$
	High- z + Newton-4	> 0.161	< 1.800	$-0.398^{+1.058}_{-0.892}$	-	-	-	$0.196^{+0.038}_{-0.038}$	$9.200^{+0.800}_{-0.800}$	$0.574^{+0.024}_{-0.024}$
	Chandra + XXL	$0.287^{+0.373}_{-0.087}$	$1.260^{+0.260}_{-0.026}$	$-0.697^{+0.187}_{-0.187}$	-	-	-	$0.232^{+0.008}_{-0.008}$	$9.020^{+0.660}_{-0.660}$	$0.576^{+0.028}_{-0.028}$
	Chandra + High- z + Newton-4	$0.349^{+0.307}_{-0.107}$	$1.365^{+0.087}_{-0.129}$	$-0.752^{+0.293}_{-0.129}$	-	-	-	$0.234^{+0.008}_{-0.008}$	$9.340^{+0.690}_{-0.690}$	$0.566^{+0.021}_{-0.021}$
	Chandra + XXX + Newton-3	$0.258^{+0.352}_{-0.088}$	$1.330^{+0.150}_{-0.050}$	$-0.670^{+0.160}_{-0.160}$	-	-	-	$0.230^{+0.007}_{-0.007}$	$9.020^{+0.630}_{-0.630}$	$0.576^{+0.020}_{-0.020}$
	SDSS-4XMM-I	> 0.387	< 1.900	$-1.175^{+0.235}_{-0.235}$	-	-	-	$0.232^{+0.007}_{-0.007}$	$8.180^{+0.630}_{-0.630}$	$0.600^{+0.020}_{-0.020}$
	SDSS-4XMM-h	> 0.376	$1.570^{+0.130}_{-0.110}$	$-1.448^{+0.348}_{-0.202}$	-	-	-	$0.203^{+0.006}_{-0.006}$	$10.230^{+0.630}_{-0.630}$	$0.535^{+0.010}_{-0.010}$
	QSO ^b	$0.367^{+0.273}_{-0.137}$	$1.385^{+0.084}_{-0.075}$	$-0.788^{+0.188}_{-0.292}$	-	-	-	$0.228^{+0.007}_{-0.007}$	$9.180^{+0.630}_{-0.590}$	$0.571^{+0.019}_{-0.019}$
	BAO + $H(z)$	$0.292^{+0.023}_{-0.023}$	$0.667^{+0.093}_{-0.093}$	$-0.014^{+0.075}_{-0.081}$	-0.075	-	$68.700^{+2.300}_{-2.300}$	-	-	-
	SDSS-4XMM	-	-	-	$0.105^{+0.555}_{-0.755}$	-	-	$0.224^{+0.005}_{-0.005}$	$7.480^{+0.420}_{-0.420}$	$0.623^{+0.014}_{-0.014}$
	SDSS-Chandra	> 0.207	-	-	< -0.063	-	-	$0.228^{+0.008}_{-0.008}$	$8.260^{+0.540}_{-0.540}$	$0.600^{+0.018}_{-0.018}$
	XXL	-	-	-	-0.212	-	-	$0.212^{+0.017}_{-0.017}$	$7.400^{+1.600}_{-1.600}$	$0.627^{+0.018}_{-0.018}$
	Chandra + Newton-3	> 0.219	-	-	< -0.078	-	-	$0.236^{+0.008}_{-0.008}$	$8.020^{+0.500}_{-0.500}$	$0.608^{+0.017}_{-0.017}$
	High- z + Newton-4	-	-	-	< -0.180	-	-	$0.198^{+0.038}_{-0.038}$	$9.260^{+1.800}_{-1.800}$	$0.575^{+0.023}_{-0.023}$
	Chandra + XXL	> 0.248	-	-	< -0.100	-	-	$0.234^{+0.008}_{-0.008}$	$8.130^{+0.500}_{-0.500}$	$0.604^{+0.019}_{-0.019}$
	Chandra + High- z + Newton-4	> 0.242	-	-	< 0.038	-	-	$0.238^{+0.008}_{-0.008}$	$7.890^{+0.500}_{-0.500}$	$0.612^{+0.017}_{-0.017}$
	Chandra + XXL + Newton-3	> 0.248	-	-	< -0.083	-	-	$0.232^{+0.008}_{-0.008}$	$7.930^{+0.470}_{-0.470}$	$0.611^{+0.017}_{-0.017}$
	SDSS-4XMM-I	> 0.234	-	-	< 0.003	-	-	$0.233^{+0.007}_{-0.007}$	$8.040^{+0.680}_{-0.680}$	$0.605^{+0.022}_{-0.022}$
	SDSS-4XMM-h	-	-	-	< 0.112	-	-	$0.207^{+0.007}_{-0.007}$	$9.490^{+0.680}_{-0.680}$	$0.560^{+0.019}_{-0.019}$
	QSO ^b	> 0.238	-	-	< 0.066	-	-	$0.232^{+0.008}_{-0.008}$	$7.650^{+0.440}_{-0.440}$	$0.620^{+0.015}_{-0.015}$
	BAO + $H(z)$	$0.282^{+0.021}_{-0.021}$	-	-	$-0.744^{+0.140}_{-0.097}$	-	$65.800^{+2.200}_{-2.500}$	-	-	-
	SDSS-4XMM	> 0.362	-	-	$-0.994^{+0.344}_{-0.216}$	< -1.300	-	$0.219^{+0.005}_{-0.005}$	$9.650^{+0.480}_{-0.480}$	$0.557^{+0.016}_{-0.016}$
	SDSS-Chandra	> 0.137	-	-	$-0.581^{+0.511}_{-0.509}$	$-0.767^{+0.757}_{+1.393}$	-	$0.237^{+0.008}_{-0.009}$	$8.910^{+0.720}_{-0.720}$	$0.579^{+0.023}_{-0.023}$
Non-flat XCDM										

Model	Data set	Ω_m	Ω_Λ^c	Ω_{k0}	ω_X	α	H_0^a	δ	β	γ
XXL	—	—	—	0.289 ^{+0.061} _{-0.059}	-0.939 ^{+0.739} _{-2.361}	—	—	0.212 ^{+0.017} _{-0.017}	7.300 ^{+1.500} _{-1.700}	0.629 ^{+0.050} _{-0.050}
Chandra + Newton-3	0.244 ^{+0.476} _{-0.104}	—	—	-0.581 ^{+0.471} _{-0.539}	-0.608 ^{+0.418} _{-1.382}	—	—	0.235 ^{+0.007} _{-0.009}	8.840 ^{+0.700} _{-0.700}	0.582 ^{+0.024} _{-0.024}
High- z + Newton-4	—	—	—	-0.154 ^{+0.904} _{-0.904}	—	—	—	0.196 ^{+0.037} _{-0.048}	9.220 ^{+1.800} _{-1.800}	0.573 ^{+0.023} _{-0.023}
Chandra + XXL	—	—	—	-0.588 ^{+0.858} _{-0.858}	-0.801 ^{+0.751} _{-1.389}	—	—	0.233 ^{+0.009} _{-0.008}	8.870 ^{+0.710} _{-0.710}	0.581 ^{+0.025} _{-0.025}
Chandra + High- z + Newton-4	0.324 ^{+0.356} _{-0.174}	—	—	-0.643 ^{+0.423} _{-0.423}	-0.892 ^{+0.632} _{-1.023}	—	—	0.235 ^{+0.009} _{-0.009}	9.250 ^{+0.820} _{-0.820}	0.569 ^{+0.021} _{-0.021}
Chandra + XXL + Newton-3	0.274 ^{+0.456} _{-0.134}	—	—	-0.603 ^{+0.463} _{-0.463}	-0.837 ^{+0.707} _{-1.203}	—	—	0.231 ^{+0.008} _{-0.008}	8.860 ^{+0.690} _{-0.690}	0.582 ^{+0.022} _{-0.022}
SDSS-4XMM-I	0.207	—	—	-0.600 ^{+0.570} _{-0.570}	< 0.300	—	—	0.233 ^{+0.007} _{-0.007}	8.250 ^{+0.720} _{-0.720}	0.598 ^{+0.024} _{-0.024}
SDSS-4XMM-h	> 0.358	—	—	-1.018 ^{+0.358} _{-0.292}	< -0.500	—	—	0.203 ^{+0.006} _{-0.006}	10.240 ^{+0.600} _{-0.600}	0.536 ^{+0.012} _{-0.012}
QSO ^b	0.324 ^{+0.325} _{-0.184}	—	—	-0.705 ^{+0.465} _{-0.465}	-0.902 ^{+0.572} _{-0.848}	—	—	0.229 ^{+0.008} _{-0.008}	9.060 ^{+0.760} _{-0.640}	0.575 ^{+0.021} _{-0.021}
BAO + $H(z)$	0.293 ^{+0.047} _{-0.027}	—	—	-0.120 ^{+0.158} _{-0.130}	-0.693 ^{+0.373} _{-0.373}	—	65.900 ^{+2.400} _{-2.400}	—	—	—
Flat ϕ CDM	SDSS-4XMM	> 0.710	—	—	—	—	—	0.225 ^{+0.005} _{-0.005}	7.290 ^{+0.390} _{-0.390}	0.630 ^{+0.013} _{-0.013}
SDSS-Chandra	> 0.281	—	—	—	—	—	—	0.238 ^{+0.008} _{-0.008}	8.200 ^{+0.540} _{-0.540}	0.601 ^{+0.018} _{-0.018}
XXL	—	—	—	—	—	—	—	0.211 ^{+0.015} _{-0.015}	7.400 ^{+0.540} _{-0.540}	0.626 ^{+0.018} _{-0.018}
Chandra + Newton-3	> 0.291	—	—	—	—	—	—	0.236 ^{+0.008} _{-0.008}	7.960 ^{+0.500} _{-0.500}	0.609 ^{+0.016} _{-0.016}
High- z + Newton-4	—	—	—	—	—	—	—	0.197 ^{+0.036} _{-0.036}	9.280 ^{+0.800} _{-0.800}	0.573 ^{+0.022} _{-0.022}
Chandra + XXL	> 0.311	—	—	—	—	—	—	0.234 ^{+0.048} _{-0.048}	8.080 ^{+0.690} _{-0.690}	0.605 ^{+0.059} _{-0.059}
Chandra + High- z + Newton-4	> 0.394	—	—	—	—	—	—	0.239 ^{+0.008} _{-0.008}	7.820 ^{+0.500} _{-0.500}	0.613 ^{+0.016} _{-0.016}
Chandra + XXL + Newton-3	> 0.321	—	—	—	—	—	—	0.232 ^{+0.007} _{-0.007}	7.850 ^{+0.470} _{-0.470}	0.612 ^{+0.016} _{-0.016}
SDSS-4XMM-I	> 0.243	—	—	—	—	—	—	0.233 ^{+0.007} _{-0.007}	7.990 ^{+0.670} _{-0.670}	0.606 ^{+0.025} _{-0.025}
SDSS-4XMM-h	> 0.471	—	—	—	—	—	—	0.207 ^{+0.006} _{-0.006}	9.470 ^{+0.580} _{-0.580}	0.560 ^{+0.022} _{-0.022}
QSO ^b	> 0.420	—	—	—	—	—	—	0.232 ^{+0.009} _{-0.009}	7.590 ^{+0.480} _{-0.440}	0.621 ^{+0.019} _{-0.019}
BAO + $H(z)$	0.266 ^{+0.023} _{-0.023}	—	—	—	1.530 ^{+0.620} _{-0.850}	65.100 ^{+2.100} _{-2.100}	—	—	—	—
Non-flat ϕ CDM	SDSS-4XMM	> 0.816	—	-0.915 ^{+0.101} _{-0.101}	—	—	—	0.223 ^{+0.005} _{-0.005}	7.820 ^{+0.420} _{-0.420}	0.612 ^{+0.014} _{-0.014}
SDSS-Chandra	> 0.369	—	—	-0.259 ^{+0.298} _{-0.298}	—	—	0.238 ^{+0.008} _{-0.008}	8.370 ^{+0.576} _{-0.576}	0.595 ^{+0.014} _{-0.014}	
XXL	—	—	—	0.008 ^{+0.431} _{-0.431}	—	—	0.211 ^{+0.016} _{-0.016}	7.400 ^{+0.576} _{-0.576}	0.627 ^{+0.049} _{-0.049}	
Chandra + Newton-3	> 0.380	—	—	-0.288 ^{+0.308} _{-0.248}	—	—	—	0.235 ^{+0.008} _{-0.008}	8.150 ^{+0.530} _{-0.530}	0.602 ^{+0.018} _{-0.018}
High- z + Newton-4	—	—	—	-0.033 ^{+0.352} _{-0.352}	—	—	—	0.197 ^{+0.036} _{-0.036}	9.290 ^{+0.530} _{-0.530}	0.572 ^{+0.022} _{-0.022}
Chandra + XXL	> 0.404	—	—	-0.313 ^{+0.253} _{-0.253}	—	—	—	0.234 ^{+0.008} _{-0.008}	8.270 ^{+0.540} _{-0.540}	0.598 ^{+0.018} _{-0.018}
Chandra + High- z + Newton-4	> 0.513	—	—	-0.723 ^{+0.347} _{-0.347}	—	—	—	0.237 ^{+0.008} _{-0.008}	8.200 ^{+0.560} _{-0.560}	0.600 ^{+0.018} _{-0.018}
Chandra + XXL + Newton-3	> 0.420	—	—	-0.329 ^{+0.249} _{-0.249}	—	—	—	0.232 ^{+0.008} _{-0.008}	8.080 ^{+0.560} _{-0.560}	0.604 ^{+0.018} _{-0.018}
SDSS-4XMM-I	> 0.265	—	—	-0.156 ^{+0.326} _{-0.326}	—	—	—	0.233 ^{+0.007} _{-0.007}	8.020 ^{+0.670} _{-0.670}	0.605 ^{+0.022} _{-0.022}
SDSS-4XMM-h	> 0.598	—	—	-0.788 ^{+0.384} _{-0.288}	—	—	—	0.206 ^{+0.006} _{-0.006}	9.650 ^{+0.680} _{-0.680}	0.553 ^{+0.018} _{-0.018}
QSO ^b	> 0.545	—	—	-0.745 ^{+0.326} _{-0.100}	-0.745 ^{+0.185} _{-0.100}	—	0.231 ^{+0.009} _{-0.007}	8.000 ^{+0.480} _{-0.440}	0.607 ^{+0.016} _{-0.016}	
BAO + $H(z)$	0.271 ^{+0.024} _{-0.028}	—	—	-0.080 ^{+0.100} _{-0.100}	1.660 ^{+0.670} _{-0.830}	65.500 ^{+2.500} _{-2.500}	—	—	—	—

^a km s⁻¹Mpc⁻¹.^b Chandra + XXL + High- z + Newton-3 + Newton-4.^c Here Ω_Λ is a derived parameter and Ω_{k0} chains are derived using the current energy budget equation $\Omega_\Lambda = 1 - \Omega_{m0} - \Omega_{k0}$ (where in the flat Λ CDM model $\Omega_{k0} = 0$). We use the PYTHON package GETDIST (Lewis 2019) to determine best-fit values and uncertainties for Ω_Λ from these chains. We also use this PYTHON package to compute the free parameters and plot the likelihoods.

For the SDSS-4XMM QSOs, beside the model- and redshift-dependent β and γ values, in the flat models especially, as shown in Fig. 1, these QSO data strongly favor currently decelerating cosmological expansion, contradicting constraints from most other cosmological data. Figure 1 also shows that even when the SDSS-4XMM constraints are consistent with currently accelerating cosmological expansion they pick out a different part of parameter space compared to what is favored by BAO + $H(z)$ data. Figure 2 shows that the lower and higher redshift halves of the SDSS-4XMM sub-sample result in somewhat different cosmological constraints.

For the SDSS-Chandra QSOs, which is the second largest sub-sample, comparing β and γ values for each of the six cosmological models, we see that these β and γ values are almost model-independent. For these QSOs, quantitative differences between β and γ values for different pairs of cosmological models are listed in Table 10. The difference between γ values ($\Delta\gamma$) from model to model ranges over $(0.04 - 0.96)\sigma$ while that between β values ($\Delta\beta$) ranges over $(0.01 - 0.99)\sigma$, both of which are almost statistically insignificant. This shows that SDSS-Chandra QSOs are standardizable via the $L_X - L_{UV}$ relation. For the XXL QSOs, which is the third largest sub-group, β and γ values are model-independent. For these QSOs, differences between β and γ values for different pair of cosmological model are listed in Table 11 and are almost negligible. This shows that the XXL sub-sample is standardizable through the $L_X - L_{UV}$ relation. Figure 3 shows that the SDSS-Chandra QSO constraints are largely consistent with those that follow from BAO + $H(z)$ data, while Fig. 4 shows that the much smaller XXL sub-group results in less-restrictive cosmological constraints that are consistent with those that follow from the BAO + $H(z)$ measurements.

We have also analysed some combinations of sub-groups to see whether these combinations have model-independent $L_X - L_{UV}$ relations and so can be used to measure cosmological model parameters. Results for β and γ for these combinations of QSOs are listed in Table 5. From this table and Table 12, for the High- z + Newton-4 combination, β and γ values do not show significant model-dependency. This small sub-sample of 36 QSOs results in weak cosmological parameter constraints, see Fig. 5. For the larger SDSS-Chandra + XXL combination of 618 QSOs, Table 13, the difference between γ values ($\Delta\gamma$) from model to model range over $(0 - 1.04)\sigma$ and that between β values ($\Delta\beta$) range over $(0.01 - 1.14)\sigma$, which are almost statistically insignificant. The cosmological constraints from this larger sub-sample are more restrictive, and largely consistent with those that follow from BAO + $H(z)$ data, see Fig. 6. For the SDSS-Chandra + Newton-3 combination, Table 14, the difference between γ values ($\Delta\gamma$) from model to model range over $(0 - 1.21)\sigma$ and that between β values ($\Delta\beta$) range over $(0.00 - 1.26)\sigma$, which are almost statistically insignificant. Figure 7 shows that the cosmological constraints from this larger sub-sample of 556 QSOs are more restrictive and largely consistent with those that follow from BAO + $H(z)$ data. For the SDSS-Chandra + XXL + Newton-3 combination of 632 QSOs, Table 15, the difference between γ values ($\Delta\gamma$) from model to model range over $(0.05 - 1.44)\sigma$ and that between β values ($\Delta\beta$) range over $(0.00 - 1.49)\sigma$, which could both be statistically significant. This means that the SDSS-Chandra + XXL and Newton-3 sub-samples might not be mutually consistent. Figure 8 shows the resulting cosmological constraints. For the SDSS-Chandra + High- z + Newton-4 combination of 578 QSOs, Table 16, the difference between γ values ($\Delta\gamma$) from model to model range over $(0.04 - 1.78)\sigma$ and that between β values ($\Delta\beta$) range over $(0.00 - 1.89)\sigma$, which could both be statistically significant. This means that the SDSS-Chandra and High- z + Newton-4 sub-samples might not be mutually consistent. The resulting joint cosmological

Table 6. $L_X - L_{UV}$ relation parameters (and δ) differences between different models for the SDSS-4XMM data.

Model vs model	$\Delta\delta$	$\Delta\gamma$	$\Delta\beta$
Flat Λ CDM vs non-flat Λ CDM	0.47σ	3.44σ	3.53σ
Flat Λ CDM vs flat XCDM	0.14σ	0.37σ	0.33σ
Flat Λ CDM vs non-flat XCDM	0.85σ	3.54σ	3.78σ
Flat Λ CDM vs flat ϕ CDM	0.00σ	0.00σ	0.00σ
Flat Λ CDM vs non-flat ϕ CDM	0.28σ	0.94σ	0.91σ
Non-flat Λ CDM vs flat XCDM	0.71σ	3.01σ	3.16σ
Non-flat Λ CDM vs non-flat XCDM	0.00σ	0.09σ	0.27σ
Non-flat Λ CDM vs flat ϕ CDM	0.85σ	3.44σ	3.57σ
Non-flat Λ CDM vs non-flat ϕ CDM	0.57σ	2.49σ	2.62σ
Flat XCDM vs non-flat XCDM	0.71σ	3.10σ	3.40σ
Flat XCDM vs flat ϕ CDM	0.14σ	0.37σ	0.33σ
Flat XCDM vs non-flat ϕ CDM	0.14σ	0.56σ	0.57σ
Non-flat XCDM vs flat ϕ CDM	0.85σ	3.54σ	3.82σ
Non-flat XCDM vs non-flat ϕ CDM	0.57σ	2.59σ	2.87σ
Flat ϕ CDM vs non-flat ϕ CDM	0.28σ	0.94σ	0.92σ

Table 7. $L_X - L_{UV}$ relation parameters (and δ) differences between different models and lower and higher redshift halves of the SDSS-4XMM data set.

Model	$\Delta\delta$	$\Delta\gamma$	$\Delta\beta$
Between SDSS-4XMM-I and SDSS-4XMM-h			
Flat Λ CDM	2.82σ	1.58σ	1.69σ
Non-flat Λ CDM	3.15σ	2.5σ	2.14σ
Flat XCDM	2.63σ	1.55σ	1.62σ
Non-flat XCDM	3.25σ	2.31σ	2.12σ
Flat ϕ CDM	2.82σ	1.58σ	1.67σ
Non-flat ϕ CDM	2.93σ	1.83σ	1.87σ

constraints are shown in Fig. 9. For the SDSS-Chandra + XXL + High- z + Newton-3 + Newton-4 combination of 668 QSOs, Table 17, the difference between γ values ($\Delta\gamma$) from model to model range over $(0.00 - 2.07)\sigma$ and that between β values ($\Delta\beta$) range over $(0.00 - 2.16)\sigma$, which could both be statistically significant. This suggests that the SDSS-Chandra + XXL and High- z + Newton-3 + Newton-4 sub-samples might not be mutually consistent. The resulting joint cosmological constraints are shown in Fig. 10.

While there are combinations of QSO sub-sets with model-independent $L_X - L_{UV}$ relations, perhaps the current best QSO $L_X - L_{UV}$ compilation for the purpose of constraining cosmological parameters is the $z \lesssim 1.5$ sub-set of about half the Lusso et al. (2020) QSOs used in Khadka & Ratra (2021) that provides relatively weak constraints which are consistent with those from better-established cosmological probes.

6 CONCLUSION

Khadka & Ratra (2021) discovered that Lusso et al. (2020) QSO data had $L_X - L_{UV}$ relation parameters that are cosmological-model as well as redshift dependent. These data are the compilation of seven different sub-samples. In this paper, we analysed these sub-groups, and some combination of sub-groups, to try to determine which QSO sub-groups are responsible for the issues pointed out in Khadka & Ratra (2021).

From our sub-sample analyses here it is clear that β and γ values for the large SDSS-4XMM sub-sample are model as well as

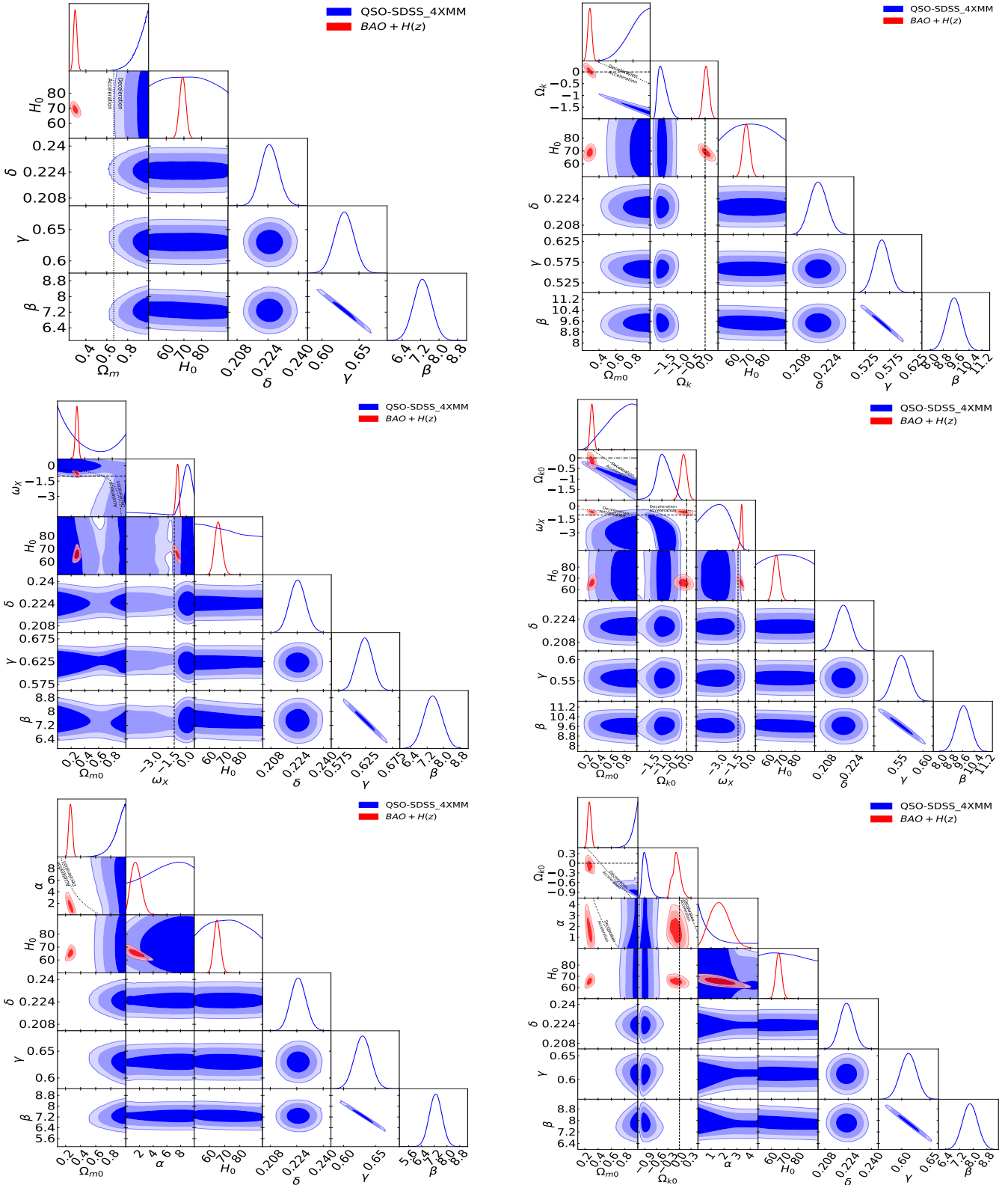


Figure 1. One-dimensional likelihood distributions and two-dimensional likelihood contours at 1σ , 2σ , and 3σ confidence levels using SDSS-4XMM (blue) and BAO + $H(z)$ (red) data for all free parameters. Left column shows the flat Λ CDM model, flat XCDM parametrization, and flat ϕ CDM model respectively. The black dotted lines in all plots are the zero acceleration lines. The black dashed lines in the flat XCDM parametrization plots are the $\omega_X = -1$ lines. Right column shows the non-flat Λ CDM model, non-flat XCDM parametrization, and non-flat ϕ CDM model respectively. Black dotted lines in all plots are the zero acceleration lines. Black dashed lines in the non-flat Λ CDM and ϕ CDM model plots and black dotted-dashed lines in the non-flat XCDM parametrization plots correspond to $\Omega_{k0} = 0$. The black dashed lines in the non-flat XCDM parametrization plots are the $\omega_X = -1$ lines.

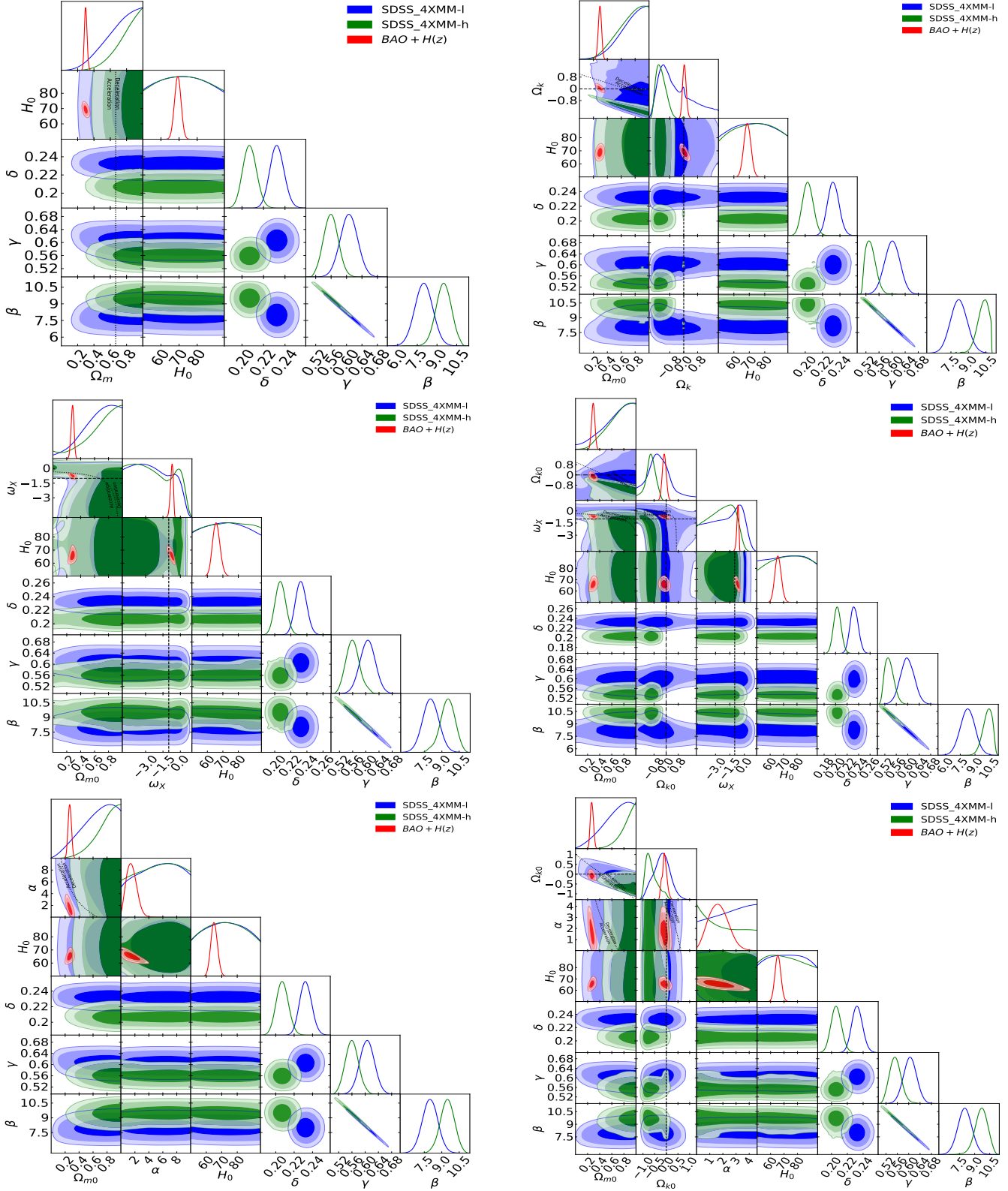


Figure 2. One-dimensional likelihood distributions and two-dimensional likelihood contours at 1σ , 2σ , and 3σ confidence levels using SDSS-4XMM-I (blue), SDSS-4XMM-h (green), and BAO + $H(z)$ (red) data for all free parameters. Left column shows the flat Λ CDM model, flat XCDM parametrization, and flat ϕ CDM model respectively. The black dotted lines in all plots are the zero acceleration lines. The black dashed lines in the flat XCDM parametrization plots are the $\omega_X = -1$ lines. Right column shows the non-flat Λ CDM model, non-flat XCDM parametrization, and non-flat ϕ CDM model respectively. Black dotted lines in all plots are the zero acceleration lines. Black dashed lines in the non-flat Λ CDM and ϕ CDM model plots and black dotted-dashed lines in the non-flat XCDM parametrization plots correspond to $\Omega_{k0} = 0$. The black dashed lines in the non-flat XCDM parametrization plots are the $\omega_X = -1$ lines.

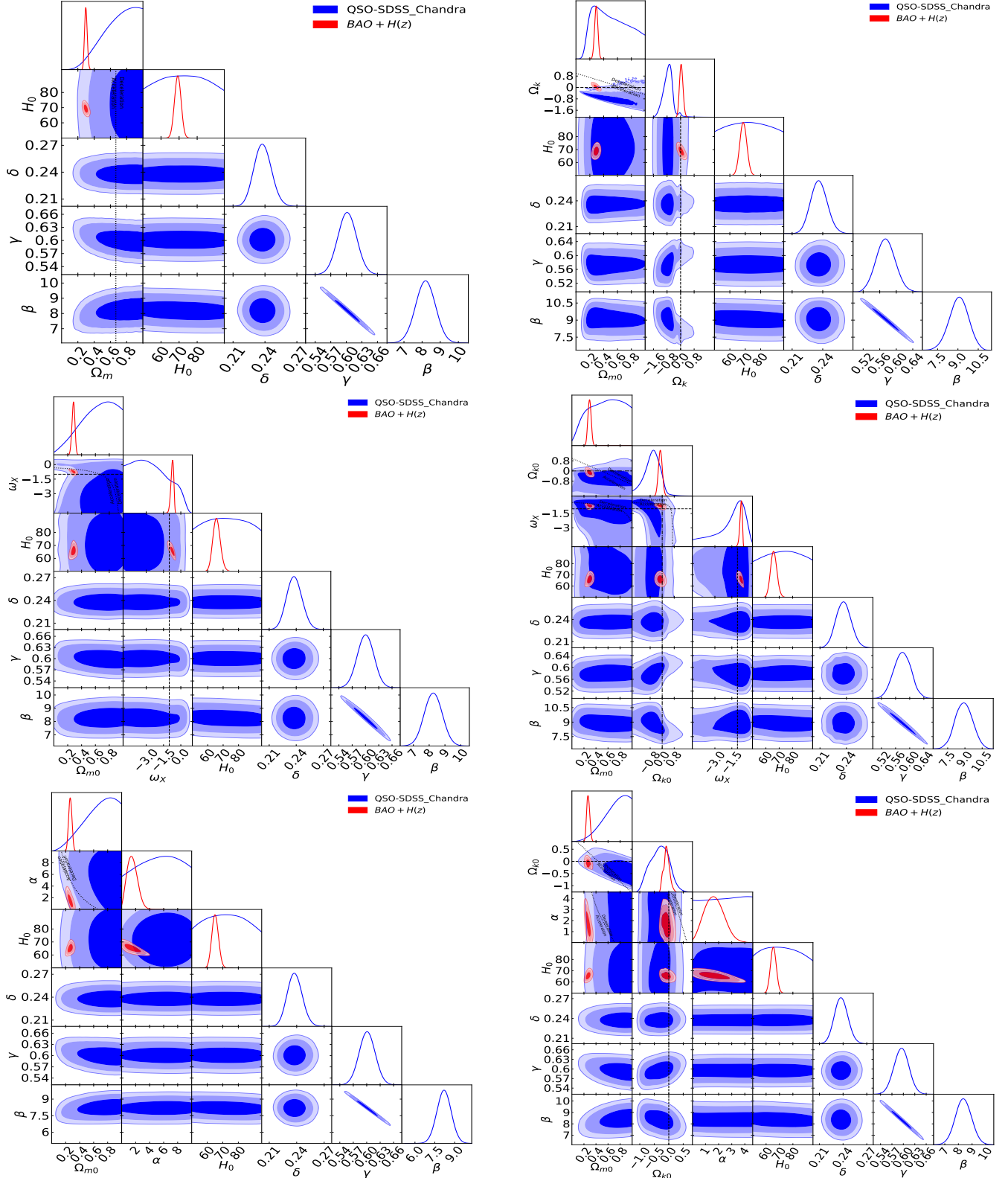


Figure 3. One-dimensional likelihood distributions and two-dimensional likelihood contours at 1σ , 2σ , and 3σ confidence levels using SDSS-Chandra (blue) and BAO + $H(z)$ (red) data for all free parameters. Left column shows the flat Λ CDM model, flat XCDM parametrization, and flat ϕ CDM model respectively. The black dotted lines in all plots are the zero acceleration lines. The black dashed lines in the flat XCDM parametrization plots are the $\omega_X = -1$ lines. Right column shows the non-flat Λ CDM model, non-flat XCDM parametrization, and non-flat ϕ CDM model respectively. Black dotted lines in all plots are the zero acceleration lines. Black dashed lines in the non-flat Λ CDM and ϕ CDM model plots and black dotted-dashed lines in the non-flat XCDM parametrization plots correspond to $\Omega_{k0} = 0$. The black dashed lines in the non-flat XCDM parametrization plots are the $\omega_X = -1$ lines.

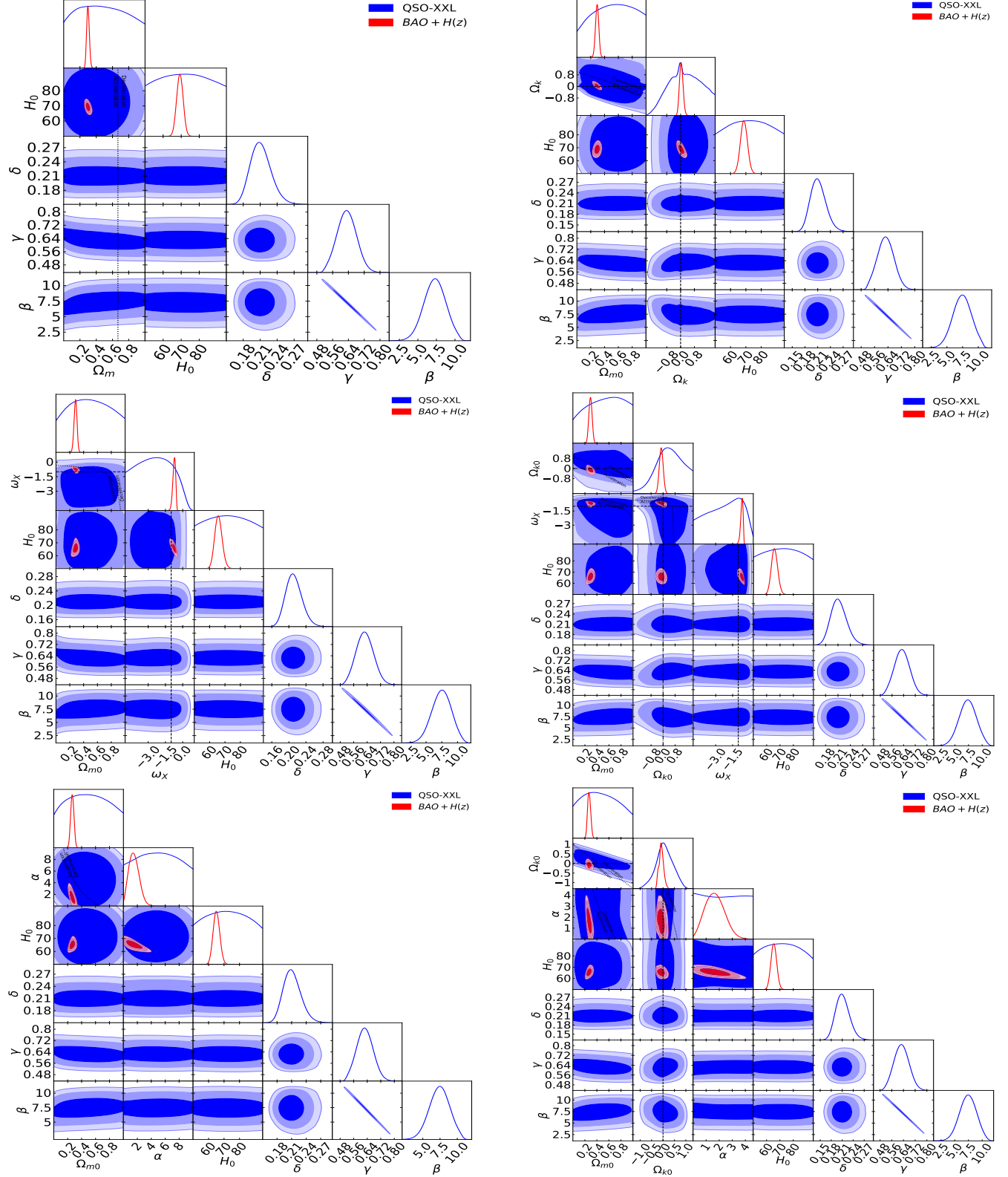


Figure 4. One-dimensional likelihood distributions and two-dimensional likelihood contours at 1σ , 2σ , and 3σ confidence levels using XXL (blue) and BAO + $H(z)$ (red) data for all free parameters. Left column shows the flat Λ CDM model, flat XCDM parametrization, and flat ϕ CDM model respectively. The black dotted lines in all plots are the zero acceleration lines. The black dashed lines in the flat XCDM parametrization plots are the $\omega_X = -1$ lines. Right column shows the non-flat Λ CDM model, non-flat XCDM parametrization, and non-flat ϕ CDM model respectively. Black dotted lines in all plots are the zero acceleration lines. Black dashed lines in the non-flat Λ CDM and ϕ CDM model plots and black dotted-dashed lines in the non-flat XCDM parametrization plots correspond to $\Omega_{k0} = 0$. The black dashed lines in the non-flat XCDM parametrization plots are the $\omega_X = -1$ lines.

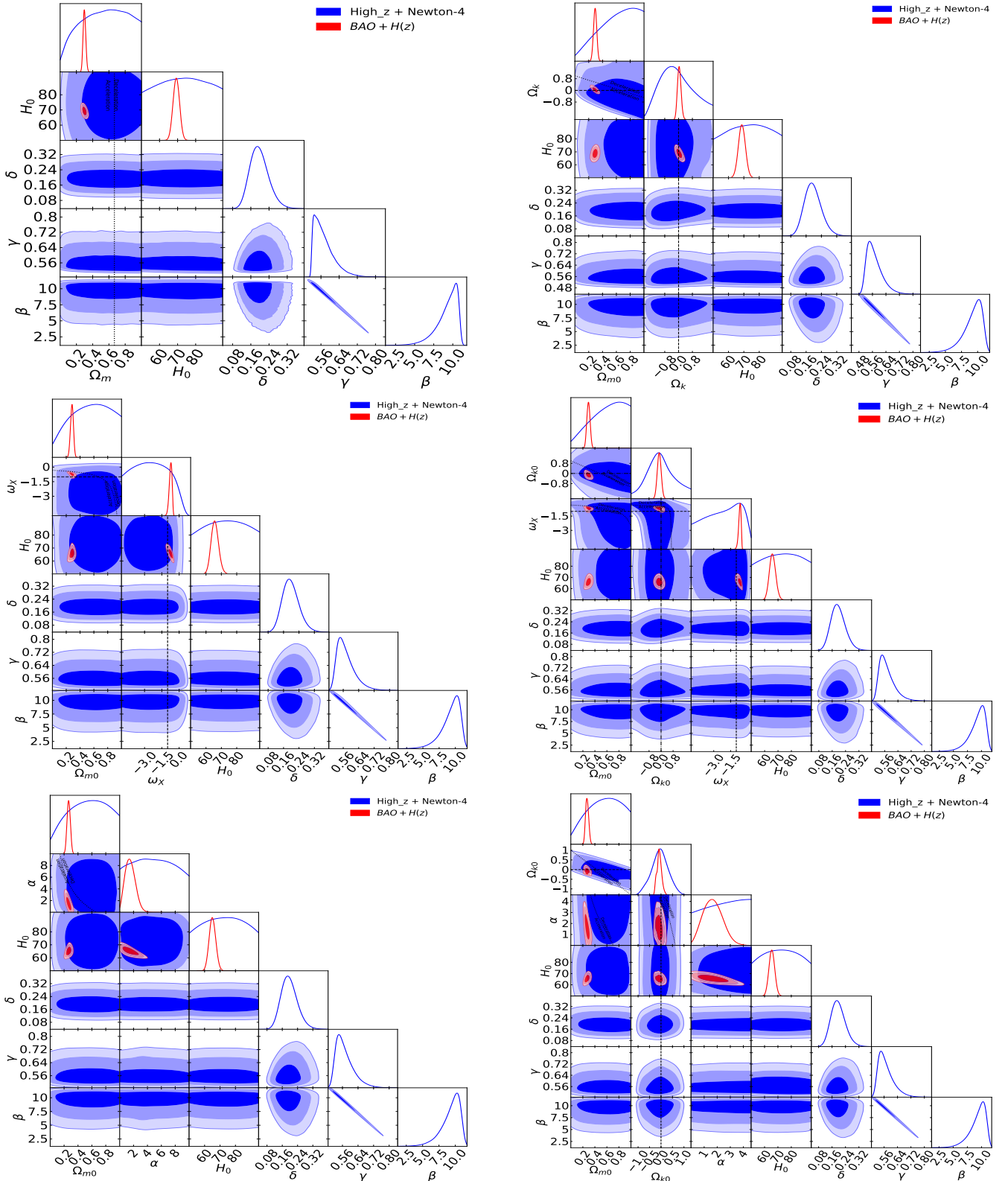


Figure 5. One-dimensional likelihood distributions and two-dimensional likelihood contours at 1σ , 2σ , and 3σ confidence levels using High- z + Newton-4 (blue) and BAO + $H(z)$ (red) data for all free parameters. Left column shows the flat Λ CDM model, flat XCDM parametrization, and flat ϕ CDM model respectively. The black dotted lines in all plots are the zero acceleration lines. The black dashed lines in the flat XCDM parametrization plots are the $\omega_X = -1$ lines. Right column shows the non-flat Λ CDM model, non-flat XCDM parametrization, and non-flat ϕ CDM model respectively. Black dotted lines in all plots are the zero acceleration lines. Black dashed lines in the non-flat Λ CDM and ϕ CDM model plots and black dotted-dashed lines in the non-flat XCDM parametrization plots correspond to $\Omega_{k0} = 0$. The black dashed lines in the non-flat XCDM parametrization plots are the $\omega_X = -1$ lines.

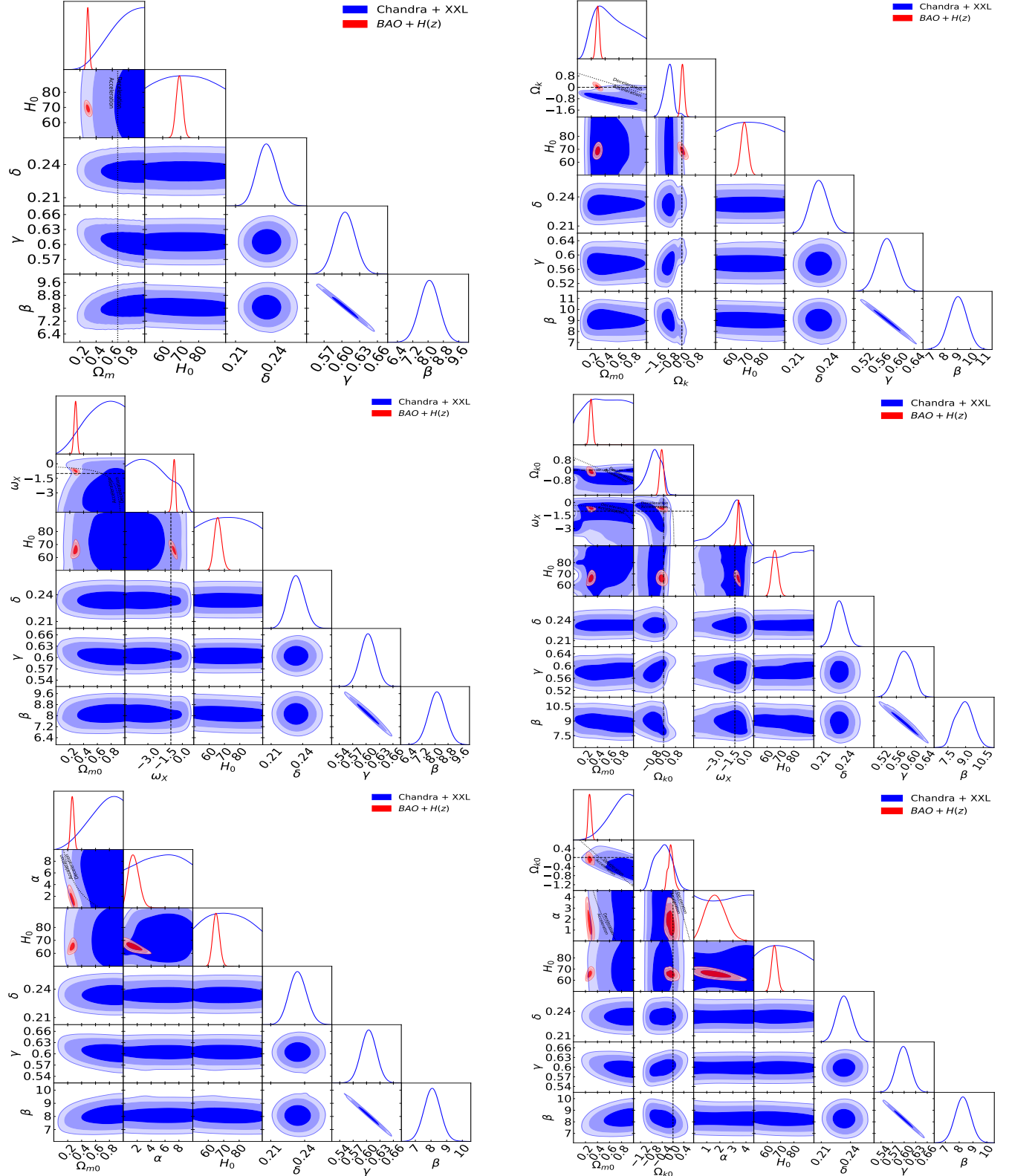


Figure 6. One-dimensional likelihood distributions and two-dimensional likelihood contours at 1σ , 2σ , and 3σ confidence levels using Chandra + XXL (blue) and BAO + $H(z)$ (red) data for all free parameters. Left column shows the flat Λ CDM model, flat XCDM parametrization, and flat ϕ CDM model respectively. The black dotted lines in all plots are the zero acceleration lines. The black dashed lines in the flat XCDM parametrization plots are the $\omega_X = -1$ lines. Right column shows the non-flat Λ CDM model, non-flat XCDM parametrization, and non-flat ϕ CDM model respectively. Black dotted lines in all plots are the zero acceleration lines. Black dashed lines in the non-flat Λ CDM and ϕ CDM model plots and black dotted-dashed lines in the non-flat XCDM parametrization plots correspond to $\Omega_{k0} = 0$. The black dashed lines in the non-flat XCDM parametrization plots are the $\omega_X = -1$ lines.

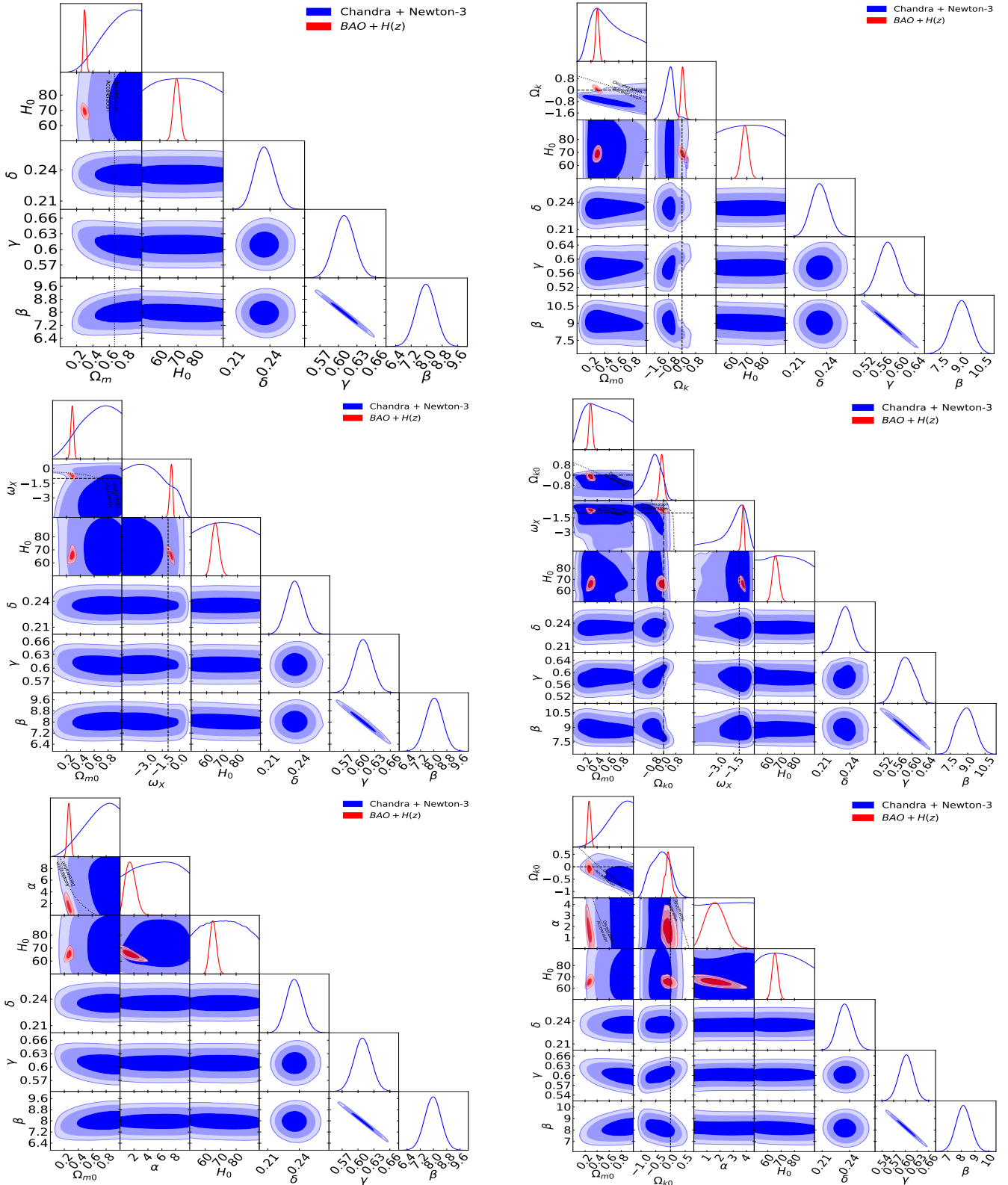


Figure 7. One-dimensional likelihood distributions and two-dimensional likelihood contours at 1σ , 2σ , and 3σ confidence levels using Chandra + Newton-3 (blue) and BAO + $H(z)$ (red) data for all free parameters. Left column shows the flat Λ CDM model, flat XCDM parametrization, and flat ϕ CDM model respectively. The black dotted lines in all plots are the zero acceleration lines. The black dashed lines in the flat XCDM parametrization plots are the $\omega_X = -1$ lines. Right column shows the non-flat Λ CDM model, non-flat XCDM parametrization, and non-flat ϕ CDM model respectively. Black dotted lines in all plots are the zero acceleration lines. Black dashed lines in the non-flat Λ CDM and ϕ CDM model plots and black dotted-dashed lines in the non-flat XCDM parametrization plots correspond to $\Omega_{k0} = 0$. The black dashed lines in the non-flat XCDM parametrization plots are the $\omega_X = -1$ lines.

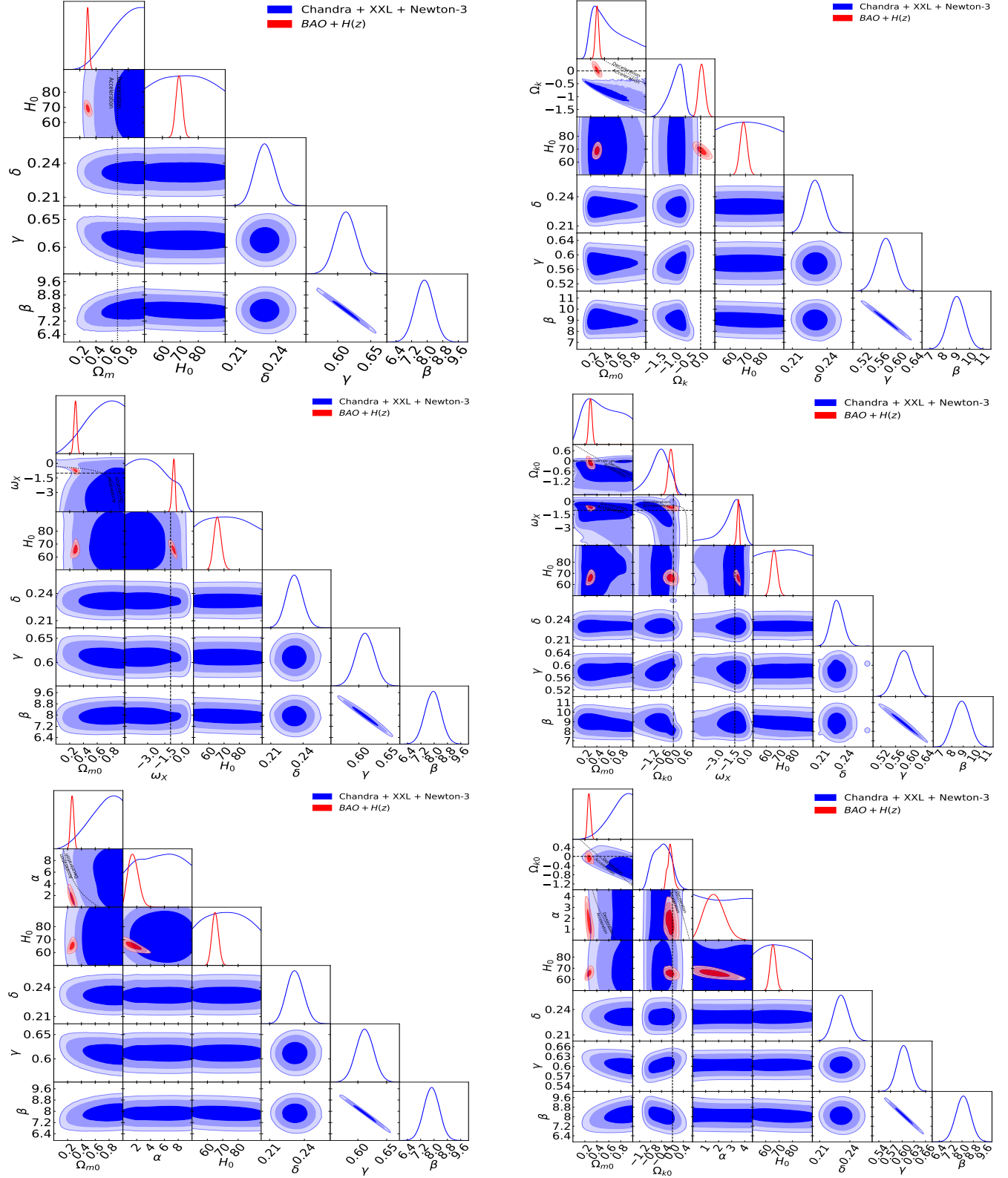


Figure 8. One-dimensional likelihood distributions and two-dimensional likelihood contours at 1σ , 2σ , and 3σ confidence levels using Chandra + XXL + Newton-3 (blue) and BAO + $H(z)$ (red) data for all free parameters. Left column shows the flat Λ CDM model, flat XCDM parametrization, and flat ϕ CDM model respectively. The black dotted lines in all plots are the zero acceleration lines. The black dashed lines in the flat XCDM parametrization plots are the $\omega_X = -1$ lines. Right column shows the non-flat Λ CDM model, non-flat XCDM parametrization, and non-flat ϕ CDM model respectively. Black dotted lines in all plots are the zero acceleration lines. Black dashed lines in the non-flat Λ CDM and ϕ CDM model plots and black dotted-dashed lines in the non-flat XCDM parametrization plots correspond to $\Omega_{k0} = 0$. The black dashed lines in the non-flat XCDM parametrization plots are the $\omega_X = -1$ lines.

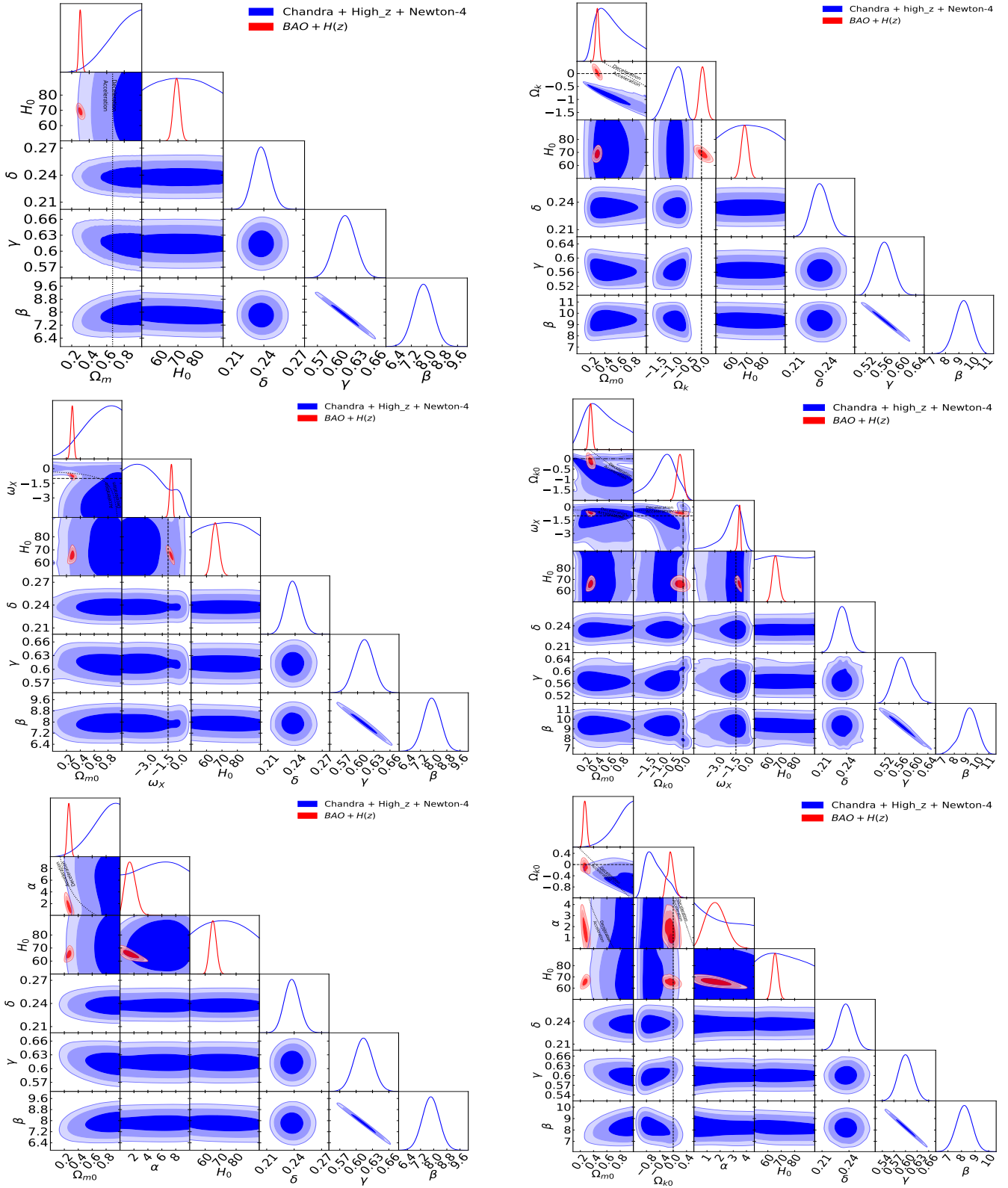


Figure 9. One-dimensional likelihood distributions and two-dimensional likelihood contours at 1σ , 2σ , and 3σ confidence levels using Chandra + High-z + Newton-4 (blue) and BAO + $H(z)$ (red) data for all free parameters. Left column shows the flat Λ CDM model, flat XCDM parametrization, and flat ϕ CDM model respectively. The black dotted lines in all plots are the zero acceleration lines. The black dashed lines in the flat XCDM parametrization plots are the $\omega_X = -1$ lines. Right column shows the non-flat Λ CDM model, non-flat XCDM parametrization, and non-flat ϕ CDM model respectively. Black dotted lines in all plots are the zero acceleration lines. Black dashed lines in the non-flat Λ CDM and ϕ CDM model plots and black dotted-dashed lines in the non-flat XCDM parametrization plots correspond to $\Omega_{k0} = 0$. The black dashed lines in the non-flat XCDM parametrization plots are the $\omega_X = -1$ lines.

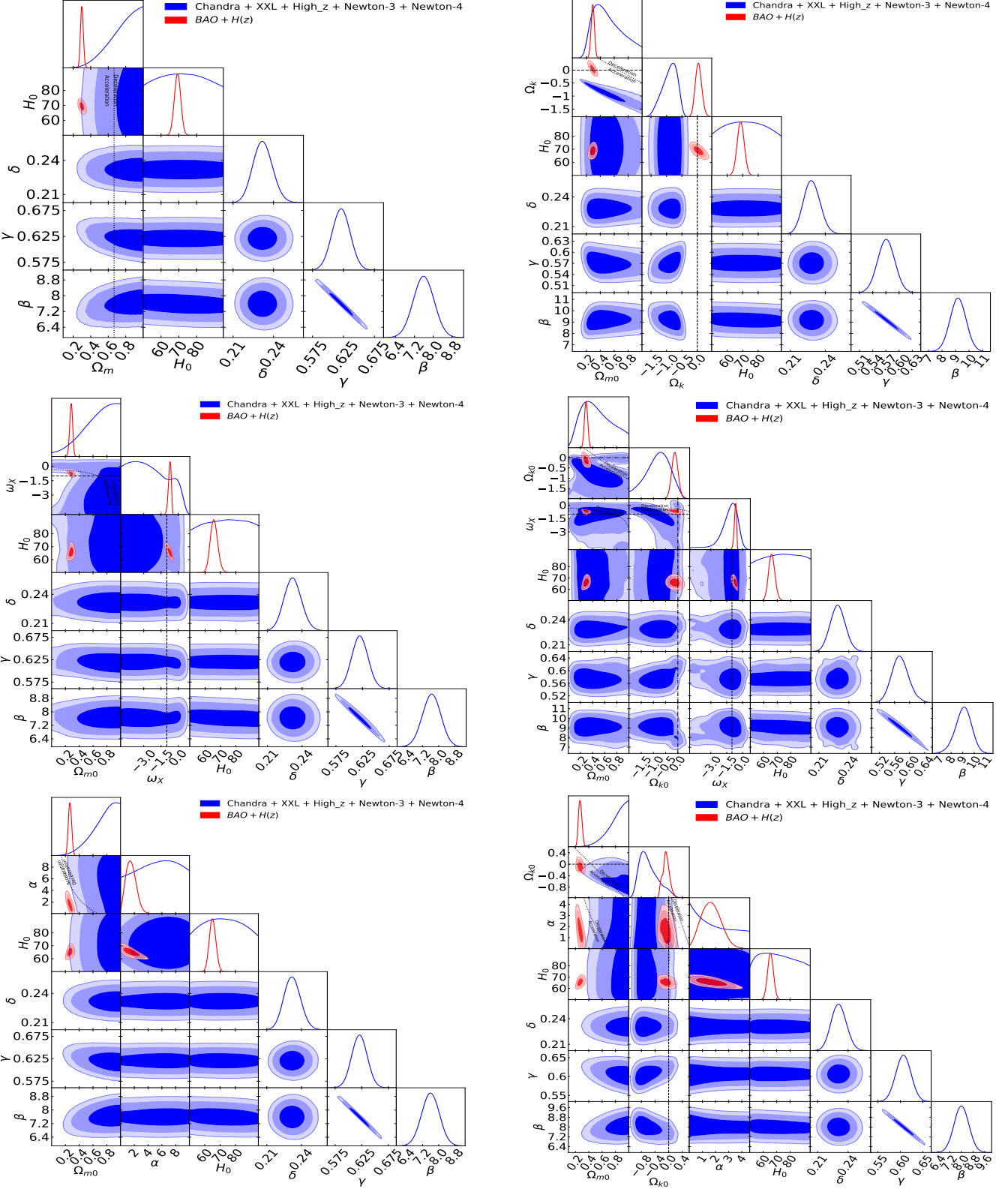


Figure 10. One-dimensional likelihood distributions and two-dimensional likelihood contours at 1σ , 2σ , and 3σ confidence levels using Chandra + XXL + High-z + Newton-3 + Newton-4 (blue) and BAO + $H(z)$ (red) data for all free parameters. Left column shows the flat Λ CDM model, flat XCDM parametrization, and flat ϕ CDM model respectively. The black dotted lines in all plots are the zero acceleration lines. The black dashed lines in the flat XCDM parametrization plots are the $\omega_X = -1$ lines. Right column shows the non-flat Λ CDM model, non-flat XCDM parametrization, and non-flat ϕ CDM model respectively. Black dotted lines in all plots are the zero acceleration lines. Black dashed lines in the non-flat Λ CDM and ϕ CDM model plots correspond to $\Omega_{k0} = 0$. The black dashed lines in the non-flat XCDM parametrization plots are the $\omega_X = -1$ lines.

Table 8. $L_X - L_{UV}$ relation parameters (and δ) differences between different models for the SDSS-4XMM-I data.

Model vs model	$\Delta\delta$	$\Delta\gamma$	$\Delta\beta$
Flat Λ CDM vs non-flat Λ CDM	0.10σ	0.18σ	0.18σ
Flat Λ CDM vs flat XCDM	0.00σ	0.030σ	0.04σ
Flat Λ CDM vs non-flat XCDM	0.00σ	0.24σ	0.25σ
Flat Λ CDM vs flat ϕ CDM	0.00σ	0.00σ	0.01σ
Flat Λ CDM vs non-flat ϕ CDM	0.00σ	0.03σ	0.02σ
Non-flat Λ CDM vs flat XCDM	0.10σ	0.15σ	0.14σ
Non-flat Λ CDM vs non-flat XCDM	0.10σ	0.05σ	0.07σ
Non-flat Λ CDM vs flat ϕ CDM	0.10σ	0.18σ	0.19σ
Non-flat Λ CDM vs non-flat ϕ CDM	0.10σ	0.15σ	0.16σ
Flat XCDM vs non-flat XCDM	0.00σ	0.22σ	0.21σ
Flat XCDM vs flat ϕ CDM	0.00σ	0.03σ	0.05σ
Flat XCDM vs non-flat ϕ CDM	0.00σ	0.00σ	0.02σ
Non-flat XCDM vs flat ϕ CDM	0.00σ	0.25σ	0.26σ
Non-flat XCDM vs non-flat ϕ CDM	0.00σ	0.22σ	0.23σ
Flat ϕ CDM vs non-flat ϕ CDM	0.00σ	0.03σ	0.03σ

redshift dependent and that the SDSS-4XMM QSOs are responsible for the cosmological-model-dependent $L_X - L_{UV}$ relation found in Khadka & Ratra (2021) for the complete Lusso et al. (2020) QSO data. This finding indicates that current SDSS-4XMM QSOs are not standardizable candles and that this issue needs to be resolved if one is to use SDSS-4XMM QSOs for cosmological purposes. We are not sure why these current SDSS-4XMM QSOs are not standardizable but possibly a more careful examination of their X-ray and UV spectra might be able to provide an explanation for this.

Additionally, when High- z + Newton-4 data are combined with other sub-samples, this results in model-dependent β and γ parameters (see Tables 16 and 17), which indicates that the higher-redshift High- z and Newton-4 sub-sample might be inconsistent with the lower-redshift sub-samples.

On the other hand, analyses of other big sub-samples, SDSS-Chandra and SDSS-Chandra + XXL, show that for these sub-samples the $L_X - L_{UV}$ relation parameters are almost independent of cosmological model. This indicates that current versions of these sub-samples can be standardized via the $L_X - L_{UV}$ relation and used for cosmological purposes. However, they provide only weak cosmological parameter constraints, constraints consistent with those determined using data obtained from better-established cosmological probes.

Given that some of the sub-samples can be standardized through the $L_X - L_{UV}$ relation, it is not impossible that a more careful study of the SDSS-4XMM sample might find an underlying issue that when corrected makes the SDSS-4XMM QSOs a valuable cosmological probe.

Additionally SDSS-Chandra + XXL QSOs, as well as reverberation-measured Mg II radius-luminosity relation QSOs (Khadka et al. 2021b), are standardizable candles and useful cosmological probes, so future detection of more such quasars will help establish QSO data as a useful probe of the as yet largely unstudied $1.5 \lesssim z \lesssim 4$ part of cosmological redshift space.

7 ACKNOWLEDGEMENTS

We thank Guido Risaliti and Salvatore Capozziello for useful discussions. This research was supported in part by DOE grant DE-

Table 9. $L_X - L_{UV}$ relation parameters (and δ) differences between different models for the SDSS-4XMM-h data.

Model vs model	$\Delta\delta$	$\Delta\gamma$	$\Delta\beta$
Flat Λ CDM vs non-flat Λ CDM	0.47σ	1.12σ	0.86σ
Flat Λ CDM vs flat XCDM	0.00σ	0.034σ	0.01σ
Flat Λ CDM vs non-flat XCDM	0.43σ	1.02σ	0.89σ
Flat Λ CDM vs flat ϕ CDM	0.00σ	0.04σ	0.04σ
Flat Λ CDM vs non-flat ϕ CDM	0.12σ	0.23σ	0.19σ
Non-flat Λ CDM vs flat XCDM	0.43σ	1.03σ	0.80σ
Non-flat Λ CDM vs non-flat XCDM	0.00σ	0.05σ	0.01σ
Non-flat Λ CDM vs flat ϕ CDM	0.47σ	1.16σ	0.89σ
Non-flat Λ CDM vs non-flat ϕ CDM	0.35σ	0.87σ	0.68σ
Flat XCDM vs non-flat XCDM	0.43σ	0.83σ	0.04σ
Flat XCDM vs flat ϕ CDM	0.00σ	0.00σ	0.02σ
Flat XCDM vs non-flat ϕ CDM	0.11σ	0.25σ	0.18σ
Non-flat XCDM vs flat ϕ CDM	0.47σ	1.07σ	0.92σ
Non-flat XCDM vs non-flat ϕ CDM	0.35σ	0.79σ	0.72σ
Flat ϕ CDM vs non-flat ϕ CDM	0.35σ	0.28σ	0.22σ

Table 10. $L_X - L_{UV}$ relation parameters (and δ) differences between different models for the SDSS-Chandra data.

Model vs model	$\Delta\delta$	$\Delta\gamma$	$\Delta\beta$
Flat Λ CDM vs non-flat Λ CDM	0.18σ	0.96σ	0.99σ
Flat Λ CDM vs flat XCDM	0.00σ	0.08σ	0.09σ
Flat Λ CDM vs non-flat XCDM	0.09σ	0.79σ	0.8σ
Flat Λ CDM vs flat ϕ CDM	0.00σ	0.04σ	0.01σ
Flat Λ CDM vs non-flat ϕ CDM	0.00σ	0.27σ	0.23σ
Non-flat Λ CDM vs flat XCDM	0.18σ	0.89σ	0.92σ
Non-flat Λ CDM vs non-flat XCDM	0.09σ	0.15σ	0.16σ
Non-flat Λ CDM vs flat ϕ CDM	0.18σ	0.92σ	0.98σ
Non-flat Λ CDM vs non-flat ϕ CDM	0.18σ	0.70σ	0.78σ
Flat XCDM vs non-flat XCDM	0.09σ	0.72σ	0.72σ
Flat XCDM vs flat ϕ CDM	0.00σ	0.04σ	0.08σ
Flat XCDM vs non-flat ϕ CDM	0.00σ	0.19σ	0.14σ
Non-flat XCDM vs flat ϕ CDM	0.09σ	0.75σ	0.79σ
Non-flat XCDM vs non-flat ϕ CDM	0.09σ	0.54σ	0.59σ
Flat ϕ CDM vs non-flat ϕ CDM	0.00σ	0.23σ	0.22σ

Table 11. $L_X - L_{UV}$ relation parameters (and δ) differences between different models for the XXL data.

Model vs model	$\Delta\delta$	$\Delta\gamma$	$\Delta\beta$
Flat Λ CDM vs non-flat Λ CDM	0.04σ	0.07σ	0.05σ
Flat Λ CDM vs flat XCDM	0.04σ	0.06σ	0.05σ
Flat Λ CDM vs non-flat XCDM	0.04σ	0.03σ	0.00σ
Flat Λ CDM vs flat ϕ CDM	0.00σ	0.07σ	0.05σ
Flat Λ CDM vs non-flat ϕ CDM	0.00σ	0.07σ	0.05σ
Non-flat Λ CDM vs flat XCDM	0.00σ	0.01σ	0.00σ
Non-flat Λ CDM vs non-flat XCDM	0.00σ	0.04σ	0.05σ
Non-flat Λ CDM vs flat ϕ CDM	0.04σ	0.00σ	0.00σ
Non-flat Λ CDM vs non-flat ϕ CDM	0.04σ	0.01σ	0.00σ
Flat XCDM vs non-flat XCDM	0.00σ	0.03σ	0.05σ
Flat XCDM vs flat ϕ CDM	0.04σ	0.01σ	0.00σ
Flat XCDM vs non-flat ϕ CDM	0.04σ	0.00σ	0.00σ
Non-flat XCDM vs flat ϕ CDM	0.00σ	0.04σ	0.05σ
Non-flat XCDM vs non-flat ϕ CDM	0.04σ	0.03σ	0.05σ
Flat ϕ CDM vs non-flat ϕ CDM	0.00σ	0.01σ	0.00σ

Table 12. $L_X - L_{UV}$ relation parameters (and δ) differences between different models for the High- z + Newton-4 data.

Model vs model	$\Delta\delta$	$\Delta\gamma$	$\Delta\beta$
Flat Λ CDM vs non-flat Λ CDM	0.03σ	0.02σ	0.03σ
Flat Λ CDM vs flat XCDM	0.00σ	0.00σ	0.01σ
Flat Λ CDM vs non-flat XCDM	0.03σ	0.03σ	0.02σ
Flat Λ CDM vs flat ϕ CDM	0.02σ	0.03σ	0.02σ
Flat Λ CDM vs non-flat ϕ CDM	0.02σ	0.05σ	0.02σ
Non-flat Λ CDM vs flat XCDM	0.03σ	0.02σ	0.03σ
Non-flat Λ CDM vs non-flat XCDM	0.00σ	0.02σ	0.01σ
Non-flat Λ CDM vs flat ϕ CDM	0.02σ	0.02σ	0.04σ
Non-flat Λ CDM vs non-flat ϕ CDM	0.02σ	0.03σ	0.05σ
Flat XCDM vs non-flat XCDM	0.03σ	0.03σ	0.02σ
Flat XCDM vs flat ϕ CDM	0.02σ	0.03σ	0.01σ
Flat XCDM vs non-flat ϕ CDM	0.02σ	0.05σ	0.02σ
Non-flat XCDM vs flat ϕ CDM	0.02σ	0.00σ	0.03σ
Non-flat XCDM vs non-flat ϕ CDM	0.02σ	0.02σ	0.04σ
Flat ϕ CDM vs non-flat ϕ CDM	0.00σ	0.02σ	0.01σ

Table 13. $L_X - L_{UV}$ relation parameters (and δ) differences between different models for the SDSS-Chandra + XXL data.

Model vs model	$\Delta\delta$	$\Delta\gamma$	$\Delta\beta$
Flat Λ CDM vs non-flat Λ CDM	0.18σ	1.04σ	1.14σ
Flat Λ CDM vs flat XCDM	0.00σ	0.04σ	0.08σ
Flat Λ CDM vs non-flat XCDM	0.09σ	0.79σ	0.92σ
Flat Λ CDM vs flat ϕ CDM	0.00σ	0.00σ	0.01σ
Flat Λ CDM vs non-flat ϕ CDM	0.00σ	0.28σ	0.27σ
Non-flat Λ CDM vs flat XCDM	0.18σ	1.01σ	1.07σ
Non-flat Λ CDM vs non-flat XCDM	0.09σ	0.15σ	0.15σ
Non-flat Λ CDM vs flat ϕ CDM	0.18σ	1.04σ	1.13σ
Non-flat Λ CDM vs non-flat ϕ CDM	0.18σ	0.77σ	0.88σ
Flat XCDM vs non-flat XCDM	0.09σ	0.76σ	0.85σ
Flat XCDM vs flat ϕ CDM	0.00σ	0.04σ	0.07σ
Flat XCDM vs non-flat ϕ CDM	0.00σ	0.24σ	0.19σ
Non-flat XCDM vs flat ϕ CDM	0.09σ	0.79σ	0.90σ
Non-flat XCDM vs non-flat ϕ CDM	0.09σ	0.55σ	0.67σ
Flat ϕ CDM vs non-flat ϕ CDM	0.00σ	0.28σ	0.26σ

Table 14. $L_X - L_{UV}$ relation parameters (and δ) differences between different models for the Chandra + Newton-3 data.

Model vs model	$\Delta\delta$	$\Delta\gamma$	$\Delta\beta$
Flat Λ CDM vs non-flat Λ CDM	0.18σ	1.19σ	1.26σ
Flat Λ CDM vs flat XCDM	0.00σ	0.04σ	0.08σ
Flat Λ CDM vs non-flat XCDM	0.09σ	0.92σ	1.00σ
Flat Λ CDM vs flat ϕ CDM	0.00σ	0.00σ	0.00σ
Flat Λ CDM vs non-flat ϕ CDM	0.09σ	0.23σ	0.26σ
Non-flat Λ CDM vs flat XCDM	0.18σ	1.15σ	1.19σ
Non-flat Λ CDM vs non-flat XCDM	0.09σ	0.18σ	0.19σ
Non-flat Λ CDM vs flat ϕ CDM	0.18σ	1.21σ	1.26σ
Non-flat Λ CDM vs non-flat ϕ CDM	0.09σ	0.91σ	1.01σ
Flat XCDM vs non-flat XCDM	0.09σ	0.88σ	0.94σ
Flat XCDM vs flat ϕ CDM	0.00σ	0.26σ	0.08σ
Flat XCDM vs non-flat ϕ CDM	0.09σ	0.24σ	0.18σ
Non-flat XCDM vs flat ϕ CDM	0.09σ	0.94σ	1.00σ
Non-flat XCDM vs non-flat ϕ CDM	0.00σ	0.67σ	0.77σ
Flat ϕ CDM vs non-flat ϕ CDM	0.09σ	0.29σ	0.26σ

Table 15. $L_X - L_{UV}$ relation parameters (and δ) differences between different models for the SDSS-Chandra + XXL + Newton-3 data.

Model vs model	$\Delta\delta$	$\Delta\gamma$	$\Delta\beta$
Flat Λ CDM vs non-flat Λ CDM	0.20σ	1.44σ	1.49σ
Flat Λ CDM vs flat XCDM	0.00σ	0.09σ	0.12σ
Flat Λ CDM vs non-flat XCDM	0.09σ	1.14σ	1.21σ
Flat Λ CDM vs flat ϕ CDM	0.00σ	0.05σ	0.00σ
Flat Λ CDM vs non-flat ϕ CDM	0.39σ	0.34σ	0.00σ
Non-flat Λ CDM vs flat XCDM	0.19σ	1.40σ	1.39σ
Non-flat Λ CDM vs non-flat XCDM	0.09σ	0.20σ	0.17σ
Non-flat Λ CDM vs flat ϕ CDM	0.20σ	1.44σ	1.49σ
Non-flat Λ CDM vs non-flat ϕ CDM	0.20σ	1.07σ	1.17σ
Flat XCDM vs non-flat XCDM	0.09σ	1.09σ	1.11σ
Flat XCDM vs flat ϕ CDM	0.00σ	0.05σ	0.12σ
Flat XCDM vs non-flat ϕ CDM	0.00σ	0.31σ	0.22σ
Non-flat XCDM vs flat ϕ CDM	0.09σ	1.13σ	1.21σ
Non-flat XCDM vs non-flat ϕ CDM	0.09σ	0.79σ	0.92σ
Flat ϕ CDM vs non-flat ϕ CDM	0.00σ	0.35σ	0.34σ

Table 16. $L_X - L_{UV}$ relation parameters (and δ) differences between different models for the SDSS-Chandra + High- z + Newton-4 data.

Model vs model	$\Delta\delta$	$\Delta\gamma$	$\Delta\beta$
Flat Λ CDM vs non-flat Λ CDM	0.38σ	1.78σ	1.89σ
Flat Λ CDM vs flat XCDM	0.00σ	0.08σ	0.10σ
Flat Λ CDM vs non-flat XCDM	0.025σ	1.67σ	1.74σ
Flat Λ CDM vs flat ϕ CDM	0.09σ	0.04σ	0.00σ
Flat Λ CDM vs non-flat ϕ CDM	0.09σ	0.57σ	0.51σ
Non-flat Λ CDM vs flat XCDM	0.35σ	1.70σ	1.80σ
Non-flat Λ CDM vs non-flat XCDM	0.08σ	0.10σ	0.10σ
Non-flat Λ CDM vs flat ϕ CDM	0.44σ	1.78σ	1.89σ
Non-flat Λ CDM vs non-flat ϕ CDM	0.27σ	1.23σ	1.35σ
Flat XCDM vs non-flat XCDM	0.25σ	1.59σ	1.66σ
Flat XCDM vs flat ϕ CDM	0.09σ	0.04σ	0.10σ
Flat XCDM vs non-flat ϕ CDM	0.09σ	0.48σ	0.41σ
Non-flat XCDM vs flat ϕ CDM	0.33σ	1.67σ	1.74σ
Non-flat XCDM vs non-flat ϕ CDM	0.17σ	1.12σ	1.22σ
Flat ϕ CDM vs non-flat ϕ CDM	0.18σ	0.54σ	0.51σ

Table 17. $L_X - L_{UV}$ relation parameters (and δ) differences between different models for the SDSS-Chandra + XXL + High- z + Newton-3 + Newton-4 data.

Model vs model	$\Delta\delta$	$\Delta\gamma$	$\Delta\beta$
Flat Λ CDM vs non-flat Λ CDM	0.40σ	2.07σ	2.16σ
Flat Λ CDM vs flat XCDM	0.00σ	0.05σ	0.10σ
Flat Λ CDM vs non-flat XCDM	0.28σ	1.78σ	1.89σ
Flat Λ CDM vs flat ϕ CDM	0.00σ	0.00σ	0.00σ
Flat Λ CDM vs non-flat ϕ CDM	0.10σ	0.64σ	0.62σ
Non-flat Λ CDM vs flat XCDM	0.38σ	2.02σ	2.08σ
Non-flat Λ CDM vs non-flat XCDM	0.09σ	0.13σ	0.13σ
Non-flat Λ CDM vs flat ϕ CDM	0.40σ	2.12σ	2.16σ
Non-flat Λ CDM vs non-flat ϕ CDM	0.30σ	1.45σ	1.54σ
Flat XCDM vs non-flat XCDM	0.27σ	1.74σ	1.82σ
Flat XCDM vs flat ϕ CDM	0.00σ	0.05σ	0.10σ
Flat XCDM vs non-flat ϕ CDM	0.09σ	0.59σ	0.53σ
Non-flat XCDM vs flat ϕ CDM	0.28σ	1.82σ	1.93σ
Non-flat XCDM vs non-flat ϕ CDM	0.19σ	1.21σ	1.35σ
Flat ϕ CDM vs non-flat ϕ CDM	0.10σ	0.66σ	0.62σ

SC0011840. Part of the computation for this project was performed on the Beocat Research Cluster at Kansas State University.

DATA AVAILABILITY

The data underlying this article are publicly available in Lusso et al. (2020).

REFERENCES

- Amati L., Guidorzi C., Frontera F., Della Valle M., Finelli F., Landi R., Montanari E., 2008, *MNRAS*, **391**, 577
- Amati L., D'Agostino R., Luongo O., Muccino M., Tantalo M., 2019, *MNRAS*, **486**, L46
- Arjona R., Nesseris S., 2021, *Phys. Rev. D*, **103**, 103539
- Avsajanishvili O., Samushia L., Arkhipova N. A., Kahnashvili T., 2015, arXiv e-prints, p. [arXiv:1511.09317](#)
- Banerjee A., Ó Colgáin E., Sasaki M., Sheikh-Jabbari M. M., Yang T., 2021, *Physics Letters B*, **818**, 136366
- Brinckmann T., Lesgourges J., 2019, *Physics of the Dark Universe*, **24**, 100260
- Cao S., Zheng X., Biesiada M., Qi J., Chen Y., Zhu Z.-H., 2017, *A&A*, **606**, A15
- Cao S., Ryan J., Ratra B., 2020, *MNRAS*, **497**, 3191
- Cao S., Ryan J., Ratra B., 2021a, arXiv e-prints, p. [arXiv:2109.01987](#)
- Cao S., Khadka N., Ratra B., 2021b, arXiv e-prints, p. [arXiv:2110.14840](#)
- Cao S., Ryan J., Khadka N., Ratra B., 2021c, *MNRAS*, **501**, 1520
- Cao S., Ryan J., Ratra B., 2021d, *MNRAS*, **504**, 300
- Chávez R., Terlevich R., Terlevich E., Bresolin F., Melnick J., Plionis M., Basilakos S., 2014, *MNRAS*, **442**, 3565
- Chen Y., Ratra B., Biesiada M., Li S., Zhu Z.-H., 2016, *ApJ*, **829**, 61
- Czerny B., et al., 2021, *Acta Physica Polonica A*, **139**, 389
- D'Agostino G., 2005, arXiv e-prints, p. [physics/0511182](#)
- DES Collaboration 2019, *Phys. Rev. D*, **99**, 123505
- Demianski M., Piedipalumbo E., Sawant D., Amati L., 2019, preprint, ([arXiv:1911.08228](#))
- Dhawan S., Alsing J., Vagnozzi S., 2021, arXiv e-prints, p. [arXiv:2104.02485](#)
- Di Valentino E., et al., 2021a, arXiv e-prints, p. [arXiv:2103.01183](#)
- Di Valentino E., Melchiorri A., Silk J., 2021b, *ApJ*, **908**, L9
- eBOSS Collaboration 2021, *Phys. Rev. D*, **103**, 083533
- Efstathiou G., Graton S., 2020, *MNRAS*, **496**, L91
- Fana Dirirsa F., et al., 2019, *ApJ*, **887**, 13
- Farooq O., Mania D., Ratra B., 2015, *Ap&SS*, **357**, 11
- Farooq O., Ranjeet Madiyar F., Crandall S., Ratra B., 2017, *ApJ*, **835**, 26
- González-Morán A. L., et al., 2019, *MNRAS*, **487**, 4669
- González-Morán A. L., et al., 2021, *MNRAS*, **505**, 1441
- Handley W., 2019, *Phys. Rev. D*, **100**, 123517
- Hu J. P., Wang Y. Y., Wang F. Y., 2020, *A&A*, **643**, A93
- Johnson J. P., Sangwan A., Shankaranarayanan S., 2021, arXiv e-prints, p. [arXiv:2102.12367](#)
- Khadka N., Ratra B., 2020a, *MNRAS*, **492**, 4456
- Khadka N., Ratra B., 2020b, *MNRAS*, **497**, 263
- Khadka N., Ratra B., 2020c, *MNRAS*, **499**, 391
- Khadka N., Ratra B., 2021, *MNRAS*, **502**, 6140
- Khadka N., Luongo O., Muccino M., Ratra B., 2021a, arXiv e-prints, p. [arXiv:2105.12692](#)
- Khadka N., Yu Z., Zajaček M., Martinez-Aldama M. L., Czerny B., Ratra B., 2021b, arXiv e-prints, p. [arXiv:2106.11136](#)
- KiDS Collaboration 2021, *A&A*, **649**, A88
- Lewis A., 2019, preprint, ([arXiv:1910.13970](#))
- Li E.-K., Du M., Xu L., 2020, *MNRAS*, **491**, 4960
- Li X., Keeley R. E., Shafieloo A., Zheng X., Cao S., Biesiada M., Zhu Z.-H., 2021, arXiv e-prints, p. [arXiv:2103.16032](#)
- Lian Y., Cao S., Biesiada M., Chen Y., Zhang Y., Guo W., 2021, *MNRAS*, **505**, 2111–2123
- Lindner M., Max K., Platscher M., Rezacek J., 2020, *J. Cosmology Astropart. Phys.*, **2020**, 040
- Lusso E., et al., 2020, *A&A*, **642**, A150
- Mania D., Ratra B., 2012, *Physics Letters B*, **715**, 9
- Martínez-Aldama M. L., Czerny B., Kawka D., Karas V., Panda S., Zajaček M., Žycki P. T., 2019, *ApJ*, **883**, 170
- Ooba J., Ratra B., Sugiyama N., 2018a, *ApJ*, **864**, 80
- Ooba J., Ratra B., Sugiyama N., 2018b, *ApJ*, **866**, 68
- Ooba J., Ratra B., Sugiyama N., 2018c, *ApJ*, **869**, 34
- Ooba J., Ratra B., Sugiyama N., 2019, *Ap&SS*, **364**, 176
- Park C.-G., Ratra B., 2018, *ApJ*, **868**, 83
- Park C.-G., Ratra B., 2019a, *Ap&SS*, **364**, 82
- Park C.-G., Ratra B., 2019b, *Ap&SS*, **364**, 134
- Park C.-G., Ratra B., 2019c, *ApJ*, **882**, 158
- Park C.-G., Ratra B., 2020, *Phys. Rev. D*, **101**, 083508
- Pavlov A., Westmoreland S., Saaidi K., Ratra B., 2013, *Phys. Rev. D*, **88**, 123513
- Peebles P. J. E., 1984, *ApJ*, **284**, 439
- Peebles P. J. E., Ratra B., 1988, *ApJ*, **325**, L17
- Perivolaropoulos L., Skara F., 2021, arXiv e-prints, p. [arXiv:2105.05208](#)
- Planck Collaboration 2020, *A&A*, **641**, A6
- Rana A., Jain D., Mahajan S., Mukherjee A., 2017, *J. Cosmology Astropart. Phys.*, **2017**, 028
- Ratra B., Peebles P. J. E., 1988, *Phys. Rev. D*, **37**, 3406
- Rezaei M., Pour-Ojaghī S., Malekjani M., 2020, *ApJ*, **900**, 70
- Risaliti G., Lusso E., 2015, *ApJ*, **815**, 33
- Risaliti G., Lusso E., 2019, *Nature Astronomy*, **3**, 272
- Ryan J., Doshi S., Ratra B., 2018, *MNRAS*, **480**, 759
- Ryan J., Chen Y., Ratra B., 2019, *MNRAS*, **488**, 3844
- Samushia L., Ratra B., 2010, *ApJ*, **714**, 1347
- Sangwan A., Tripathi A., Jassal H. K., 2018, arXiv e-prints, p. [arXiv:1804.09350](#)
- Scolnic D. M., et al., 2018, *ApJ*, **859**, 101
- Singh A., Sangwan A., Jassal H. K., 2019, *J. Cosmology Astropart. Phys.*, **2019**, 047
- Sinha S., Banerjee N., 2021, *J. Cosmology Astropart. Phys.*, **2021**, 060
- Solà Peracaula J., de Cruz Pérez J., Gómez-Valent A., 2018, *MNRAS*, **478**, 4357
- Solà Peracaula J., Gómez-Valent A., de Cruz Pérez J., 2019, *Physics of the Dark Universe*, **25**, 100311
- Speri L., Tamanini N., Caldwell R. R., Gair J. R., Wang B., 2021, *Phys. Rev. D*, **103**, 083526
- Ureña-López L. A., Roy N., 2020, *Phys. Rev. D*, **102**, 063510
- Vagnozzi S., Di Valentino E., Gariazzo S., Melchiorri A., Mena O., Silk J., 2020, arXiv e-prints, p. [arXiv:2010.02230](#)
- Vagnozzi S., Pacucci F., Loeb A., 2021a, arXiv e-prints, p. [arXiv:2105.10421](#)
- Vagnozzi S., Loeb A., Moresco M., 2021b, *ApJ*, **908**, 84
- Velasquez-Toribio A. M., Fabris J. C., 2020, *European Physical Journal C*, **80**, 1210
- Wang J. S., Wang F. Y., Cheng K. S., Dai Z. G., 2016, *A&A*, **585**, A68
- Wang F. Y., Hu J. P., Zhang G. Q., Dai Z. G., 2021, arXiv e-prints, p. [arXiv:2106.14155](#)
- Wei J.-J., 2018, *ApJ*, **868**, 29
- Wei J.-J., Melia F., 2020, *ApJ*, **888**, 99
- Yang T., Banerjee A., Ó Colgáin E., 2020, *Phys. Rev. D*, **102**, 123532
- Yu H., Ratra B., Wang F.-Y., 2018, *ApJ*, **856**, 3
- Yu Z., et al., 2021, arXiv e-prints, p. [arXiv:2103.01973](#)
- Zajaček M., et al., 2021, *ApJ*, **912**, 10
- Zhai Z., Blanton M., Slosar A., Tinker J., 2017, *ApJ*, **850**, 183
- Zhao D., Xia J.-Q., 2021, arXiv e-prints, p. [arXiv:2105.03965](#)
- Zheng X., Cao S., Biesiada M., Li X., Liu T., Liu Y., 2021, *Science China Physics, Mechanics, and Astronomy*, **64**, 259511

This paper has been typeset from a TeX/LaTeX file prepared by the author.